Comparing the radiative effects of the anthropogenic aerosol emissions from Chile and Mexico

Tuuli Miinalainen[1], Harri Kokkola[2], Kari E. J. Lehtinen[1,2]and Thomas Khn[1,2]

[1]Department of Applied Physics, University of Eastern Finland (UEF), Kuopio, Finland
[2]Atmospheric Research Centre of Eastern Finland, Finnish Meteorological Institute (FMI), Kuopio, Finland

Key Points:

- Aerosol emission mitigation in different countries and regions can affect the atmospheric radiative balance differently
- When accounting for co-emitted pollutants, black carbon mitigation results in a positive effective radiative forcing.
- Global average effective radiative forcing per emitted unit mass of sulfur dioxide in Chile and Mexico is much higher than in China.

Corresponding author: Tuuli Miinalainen, `tuuli.miinalainen@uef.fi`

Abstract

There has been growing interest in the potential of short-lived climate forcer (SLCF) mitigation to reduce near-term global warming. Black carbon (BC) is a SLCF that is known to warm the climate by absorbing insolation and to affect the radiative balance indirectly by altering cloud properties. We used an aerosol-climate model to study the climatic effects of the anthropogenic aerosol emissions of BC, organic carbon (OC) and sulfur dioxide (SO_2) from Chile and Mexico. Limiting our analysis to areas where these emissions had notable effects on both aerosol and clouds, we found that the total radiative effects of anthropogenic aerosol emissions are different for Chile and Mexico. This was explained by differences in aerosol emission strengths, their spatial distribution and differences in orography and meteorology in these two countries. Especially the radiative forcing for Chilean emissions was influenced by the persistent stratocumulus cloud deck west of Chile. The removal of OC and SO_2 emissions caused a positive effective radiative forcing (ERF), while the removal of BC emissions caused a positive ERF for Chile, but a negative ERF for Mexico. When accounting for co-emission of other aerosol compounds, reduction of BC emission led to positive ERF in both countries. Compared to China, the removal of all anthropogenic SO_2 emissions in Chile and Mexico caused a much larger global average ERF per emitted unit mass of SO_2.

1 Introduction

Short-lived climate forcers (SLCFs) are compounds that originate either from natural sources or human activity. In broad terms, SLCFs are atmospheric compounds that can have a substantial effect on the climate and global warming, but have a relatively short atmospheric lifetime of a few days to a decade compared to long-lived greenhouse gases (e.g. carbon dioxide) which can have a lifetime of hundreds of years. SLCFs include both gaseous compounds such as methane and hydrofluoro carbons, and aerosols such as black carbon (BC), organic carbon (OC) and sulfate (SO_4) (Stohl et al., 2015; UNEP, 2011).

A large part of these pollutants, for instance BC and methane, are attributed a warming effect on the climate (S. J. Smith & Mizrahi, 2013). In addition, SLCFs are one source of air pollution which has become a central issue in most of the metropolitan areas worldwide (Krzyzanowski et al., 2014). Recently, Burnett et al. (2018) suggested that outdoor particulate air pollution could be attributable to 8.9 million deaths globally in 2015, whereas some previous estimates have been between 2 to 4 million (Silva et al., 2013; WHO, 2019). Consequently, SLCF mitigation is seen as an attractive option to bring near-term benefits for better local air quality and 'buying time' for adapting to global warming (Bowerman et al., 2013; CCAC & UNEP, 2016).

BC is a SLCF that is assumed to have a major role in global warming (AMAP, 2015; Bond et al., 2013). Typically, BC emissions are emitted during combustion processes, for example from residential heating with biomass and from vehicle engines. Natural processes, e.g. forest fires and volcanic eruptions, release substantial amounts of BC into the air as well (Bond et al., 2013). As a strongly light-absorbing substance, BC alters the Earth's radiation budget by absorbing solar radiation and thereby heating the atmosphere. The absorption or scattering of the solar radiation by atmospheric constituents is referred to as direct radiative effect (DRE). The DRE due to BC has been shown to enhance global warming, especially in the Arctic region (AMAP, 2015; W. J. Collins et al., 2013; Sand et al., 2013, 2016).

Besides direct effects, BC affects the radiative balance through so-called semi-direct and indirect effects. For instance, deposited BC darkens both snow and ice cover and thereby reduces the albedo of reflective surfaces.(AMAP, 2011) This in turn increases the amount of solar radiation absorbed by snow and ice, and diminishes the back-reflected portion of the solar insolation, which results in warming (Hansen & Nazarenko, 2004).

Furthermore, BC can impact the radiative balance indirectly by altering cloud properties. By acting as cloud condensation nuclei (CCN), BC particles can increase the cloud droplet number concentration, which changes cloud reflectivity (Twomey effect, (Twomey, 1977)). Furthermore, BC particles can impact the lifetime of clouds, cause cloud burn-off, and even can change the planetary boundary layer (PBL) height by altering the vertical heating rate in the atmosphere (Ding et al., 2016). Apart from affecting cloud properties, a change in PBL height also can increase air pollution at the surface (Ding et al., 2016). As BC radiative forcing depends strongly on the altitude of BC particles (Ban-Weiss et al., 2012; Flanner, 2013), the surface temperature responses to changes in atmospheric BC concentrations are highly complex (Yang et al., 2019).

Along BC, combustion processes release various other aerosol compounds to the atmosphere. Here we consider OC and sulfate since they are the most common co-emitted aerosol species of BC (Lamarque et al., 2010), and are known to have a strong radiative effect. Unlike BC, both OC and sulfate particles are known to cool the atmosphere, due to the scattering of the solar radiation back to space (direct effect). Like BC, sulfate and OC alter clouds indirectly, increasing their cooling potential (Boucher et al., 2013). In many regions, these indirect effects of sulfate and OC have been found to even out-weigh the direct positive radiative forcing of BC (W.-T. Chen et al., 2010; Khn et al., 2020). Although the combined indirect effects of aerosol particles are generally thought to result in a cooling of the atmosphere, they are still quite poorly understood and many of the estimates include substantial uncertainty. (Bellouin et al., 2020; Koch & Del Genio, 2010; Stjern et al., 2017; Yang et al., 2019).

Whether aerosol particles will have an overall warming or cooling effect depends on various other factors in additions to their chemical composition, e.g. on the spatial and vertical location of the aerosol, since the magnitude and sign of the aerosol radiative effect depend on surface and cloud characteristics. Furthermore, differences in the composition of emitted aerosol and oxidative conditions can have a strong influence on the direct radiative effects of aerosol particles (Paulot et al., 2018). Therefore, the climatic impacts of aerosol emissions can differ greatly between different countries (Aamaas et al., 2016).

The aim of this study is to examine the climatic effects of the anthropogenic aerosol emissions from Chile and Mexico. As a part of the multidisciplinary ERC project ClimaSlow (*ClimaSlow*, 2017), this study was motivated by the national climate programs of the two countries. Both Chile and Mexico have announced ambitious goals for BC mitigation: Mexico declared a mitigation target of 51 % BC emission reduction by the year 2030 (SEMARNAT & INECC, 2016). Similarly, being one of the first nations, Chile has included SLCF mitigation in its national determined contribution (NDC) for the Paris agreement and has recently announced the unconditional aim of reducing its BC emissions by 25 % by 2030(*Chile's Nationally Determined Contribution (NDC), Update 2020*, 2020). Moreover, Chile and Mexico are interesting targets of analysis due to their closeness to the equator, as the insolation is close to maximum in this region, which magnifies the radiative effects of the aerosol. Furthermore, the climate of the Northern coast of Chile is partly dominated by a semi-persistent stratocumulus (Sc) deck (Abel et al., 2010; Huneeus et al., 2006; Klein & Hartmann, 1993; Wood et al., 2011). This Sc deck has a significant impact on the Earth's radiation budget, as these low-level clouds strongly reflect solar radiation (Hartmann et al., 1992; Wood, 2012) and are very susceptible to changes in aerosol concentrations (G. Chen et al., 2015). Compared to clear-sky conditions, these type of clouds change the radiative forcing potential of anthropogenic aerosol drastically. A similar, but weaker cloud deck exists over the Pacific, west of Mexico (Muhlbauer et al., 2014; Wood, 2012).

Mena-Carrasco et al. (2014) studied the regional climate effects of Chilean anthropogenic aerosol emissions by using the regional climate model WRF-Chem. Simulating the period from October to November 2008, they concluded that the radiative effects of

the emissions vary greatly according to the regional emission profile: in coastal Chile the dominating SO_2 emissions caused local cooling, whereas in the densely populated central Chile the BC emissions resulted in local warming.(Mena-Carrasco et al., 2014) Furthermore, Huneeus et al. (2006) reported that sulfur emissions from northern Chile might affect the properties of the local Sc clouds during strong easterly wind episodes.

In this article, we study the climatic effects of anthropogenic BC, OC and sulfur dioxide SO_2 emissions that originate from Chile and Mexico, by using the global aerosol-climate model ECHAM-HAMMOZ (Kokkola et al., 2018; Schultz et al., 2018; Tegen et al., 2019). Our main focus was to analyze the radiative effects of these emissions and to separate the direct, semi-direct and indirect contribution. We analysed where the emissions originating from Chile and Mexico are transported to and how they affect aerosol concentrations relative to the clouds in the model. This helped us identify regions where Chilean and Mexican aerosol has the largest potential to interact with radiation or to affect cloud properties. As the anthropogenic emissions analyzed here are quite small compared to the global total, we mainly restricted our analysis to the regions that are most affected by these emissions. To put the radiative effects of Chile and Mexico into global context, we also compared them to the radiative effects due to Chinese SO_2 emissions, which are one of the highest in the world for a single country (Li et al., 2017).

2 Methods

2.1 ECHAM-HAMMOZ

We conducted all simulations with the aerosol-climate model ECHAM6.3.0-HAM2.3 (ECHAM-HAMMOZ). In ECHAM-HAMMOZ, the atmospheric general circulation model ECHAM (Roeckner et al., 2003; Stevens et al., 2013) is coupled with the aerosol module HAM (Kokkola et al., 2018; Stier et al., 2005; Tegen et al., 2019). The HAM module includes the most relevant aerosol species: BC, OC, SO_4, mineral dust and sea salt. Further, the detailed representation for aerosol is achieved by coupling the sectional SALSA2.0 aerosol micro-physics module (Kokkola et al., 2018) to the model. The SALSA discretizes the aerosol size distribution into 10 size sections, which provides an accurate and computationally efficient platform for resolving aerosol-atmosphere interactions (Kokkola et al., 2018). The grid resolution used for this study was T63L47, which corresponds to approximately $1.9\,^\circ \times 1.9^\circ$ horizontal resolution, and 47 vertical layers up to 0.01 hPa (approximately 80 km altitude).

In ECHAM-HAMMOZ, 97.5 % of the anthropogenic sulfur emissions enter the atmosphere as gas (SO_2), while 2.5 % of the SO_2 total emission mass is converted directly to sulfate particles (SO_4). When SO_2 gets oxidized in the atmosphere, it forms H_2SO_4, which then forms sulfate aerosol through new particle formation or condensation onto existing aerosol particles.

2.2 Anthropogenic aerosol emissions

For the global anthropogenic aerosol emissions of BC, OC and SO_2, we used the ECLIPSE V6a emission inventory (Klimont, 2019), which was designed with the integrated assessment model GAINS (Amann et al., 2011). The spatial emission fields were re-gridded to the ECHAM-HAMMOZ model resolution (T63, approx. $1.9\,^\circ \times 1.9^\circ$). The anthropogenic emission strengths are presented in Table 1. As can be seen, the contributions from Chile and Mexico to the global total emissions are rather small: less than 0.6 % for Chile, and 1.4 % for Mexico.

The population density of Mexico is approximately three times higher than of Chile, and this might be one of the reasons why the Mexican per capita emissions are lower compared to the Chilean ones. However, the emissions per km^2 are higher than the global

	Chile	Mexico	China	Global
BC ($kt\,yr^{-1}$)	23.36 (0.38 %)	82.21 (1.35 %)	1127.79 (18.47 %)	6107.00
OC ($kt\,yr^{-1}$)	39.64 (0.32 %)	165.13 (1.35 %)	2114.87 (17.32 %)	12 208.96
SO_2 ($kt\,yr^{-1}$)	358.01(0.57 %)	515.66 (0.82 %)	15018.67 (23.81 %)	63064.54
BC (kg/capita)	1.30	0.67	0.82	0.83
OC (kg/capita)	2.21	1.36	1.54	1.66
SO_2 (kg/capita)	19.92	4.23	10.95	8.59
BC ($kg\,km^{-2}$)	30.89	41.85	117.93	46.25
OC ($kg\,km^{-2}$)	52.42	84.06	221.15	92.46
SO_2 ($kg\,km^{-2}$)	473.50	262.50	1570.51	477.59

Table 1. ECLIPSEV6a current legislation (CLE) scenario, the annual mean anthropogenic emissions for the year 2015 for Chile, Mexico, China and the entire globe. The emissions due to shipping and aviation are not included. The percentage of the global total is shown in parentheses. The population and surface area statistics for year 2015 for the per capita and per km^2 values were retrieved from the Wold Bank database (World Bank, 2020).

averages. For Chile, the emissions per km^2 are below the global average due to Chile's relatively large surface area including deserts and sparsely inhabited areas. The Chinese SO_2 emissions stand out, even when normalized by population or by surface area, and the emissions per km^2 are three times higher than the global average.

The major sources of BC emissions are the domestic sector and traffic (Cruz-Núñez, 2014), and a large part of Mexican BC originates from urban metropolitan areas that are located on elevated territory. For instance, the altitude of Mexico City is over 2200 m, and Guadalajara and Monterrey are located at altitudes of 1500 m and 500 m, respectively. In contrast, SO_2 emissions are distributed spatially more evenly within industrial operators and the energy sector. For Chile, Santiago and the regions south of Santiago are the most crucial BC and OC emission sources (Molina et al., 2015), whereas most SO_2 originates from northern Chile (Mena-Carrasco et al., 2014), with the strongest sources being the copper industry and energy production.

2.3 Experiment design

In order to estimate the maximum radiative effect of the anthropogenic aerosol emissions from Chile and Mexico, we conducted altogether seven simulations. In order to be able to study the effects of each substance individually, we performed separate simulations where always one of the substances was removed from the emissions inventory of Chile and Mexico. Additionally, to study the impacts of co-emitted species due to BC mitigation, we performed one further simulation where BC and OC emissions were reduced simultaneously.

Note that, because Chile and Mexico are separated by the inter-tropical convergence zone, the aerosol plumes originating from these two countries do not overlap and their individual effects can thus be studied using results from the same simulation. The differences between simulations carried out in this study are presented in Table 2.3.

Simulation	Emissions	Meteorology
FREE_WIND	Full representation of all anthropogenic aerosol emissions	freely evolving wind and pressure fields
BASE	Full representation of all anthropogenic aerosol emissions	nudged towards FREE_WIND wind fields
NO_SO2	Identical to BASE, but anthropogenic SO_2 emissions from Chile and Mexico removed	nudged towards FREE_WIND wind fields
NO_BC	Identical to BASE, but anthropogenic BC emissions from Chile and Mexico removed	nudged towards FREE_WIND wind fields
NO_OC	Identical to BASE, but anthropogenic OC emissions from Chile and Mexico removed	nudged towards FREE_WIND wind fields
MITIG	Identical to BASE, but 50 % of anthropogenic BC emissions and 40 % of anthropogenic OC emissions from Chile and Mexico removed	nudged towards FREE_WIND wind fields
NO_SO2_china	Identical to BASE, but anthropogenic SO_2 emissions from China removed	nudged towards FREE_WIND wind fields

Table 2. The emission and meteorology configurations for the performed simulations

The simulation FREE_WIND was used to generate wind fields to which all other simulations could be nudged. By doing this, we aimed to minimize the effect of model dynamics on aerosol radiative effects, as discussed later on. In FREE_WIND, the model meteorology was allowed to evolve freely and only sea surface temperature (SST) and sea ice cover (SIC) were fixed to climatological monthly mean values of the years 2000 to 2015, by using the results from the PCMDIs (Program for Climate Model Diagnosis & Intercomparison) Atmospheric Model Inter-comparison Project (Taylor et al., 2012).

Except for the FREE_WIND simulation, the global wind patterns and surface pressure fields for rest of the simulations were nudged towards prescribed fields obtained from FREE_WIND using a Newtonian relaxation scheme (Zhang et al., 2014). Atmospheric temperature and dry static energy were allowed to evolve freely.

The reference simulation (**BASE**) was modeled using all aerosol emissions turned on. Furthermore, we conducted three simulations that were otherwise identical to BASE but the anthropogenic aerosol emissions originating from Chile and Mexico were removed, separately for BC (**NO_BC**), OC (**NO_OC**) and SO_2 (**NO_SO2**).

Additionally, as BC and OC are usually co-emitted species, we also wanted to analyze the effects of reducing BC and OC simultaneously. To this end we performed a perturbed simulation (**MITIG**) where the anthropogenic BC and OC emissions from Chile and Mexico where decreased by 50 % and 40 %, respectively. This was motivated by the Mexican mitigation targets for BC. The reduction percentage for OC (40 %) was estimated based on the emission scenarios BASELINE and MITIGATE of the ECLIPSEV5a (Stohl et al., 2015) emission scenarios, where a 1 % reduction in anthropogenic BC emissions results in a reduction in OC emissions of approximately 0.8 %. Additionally, our aim was to compare the radiative effects of the Chilean and Mexican emissions to those of Chinese SO_2 emissions. Therefore, we performed a similar simulation without the anthropogenic SO_2 emissions originating from China (**NO_SO2_china**).

Each simulation was run for 10 years, repeating the same aerosol emissions for the year 2015 plus a one year spin-up period. The forest fire and biomass burning emissions were taken from the GFAS emission inventory (Kaiser et al., 2012), using the monthly mean values for the years 2000 to 2016. The emissions for the aviation sector were kept fixed for all simulations, and they were retrieved from the Emissions for Atmospheric Chemistry and Climate Model Intercomparison Project (ACCMIP) database (Lamarque et al., 2010) for the year 2015, using the Representative Concentration Pathway (RCP) 4.5 scenario (Thomson et al., 2011; van Vuuren et al., 2011). In addition, we used fixed ECLIPSEV6a CLE emissions for the year 2015 for the international shipping emissions in all of the simulations. The greenhouse gas concentrations were set to fixed uniform global values, whereas the ozone and OH concentrations were taken from reanalysis data (described in (Inness et al., 2013)).

2.4 Radiative forcing calculations

In ECHAM-HAMMOZ, the aerosol direct radiative effect (DRE) is calculated according to W. D. Collins et al. (2006) by using a double-call with and without aerosol to the radiation calculation routine. The aerosol direct radiative forcing (RF_A) is then calculated as the difference in DRE between the perturbed simulation and the reference simulation (BASE) (Ghan, 2013).

The total effect on the Earth's radiation balance induced by a substance is estimated using the effective radiative forcing (ERF) concept (Boucher et al., 2013; Lohmann et al., 2010; Mülmenstädt et al., 2019; C. J. Smith et al., 2018) which includes direct, semi-direct and indirect radiative effects of aerosol. The ERF is calculated as the difference of the net radiative flux at the top of the atmosphere (TOA) between a perturbed simulation and the reference simulation.

Usually, ERF is computed using simulations with a freely evolving meteorology, but with fixed SST and SIC. However, the freely evolving meteorology introduces substantial variation in ERF, which may be larger than the actual ERF signal (e.g. (AMAP, 2015; Khn et al., 2020)), especially if the analysed region is small, as it is in our study. In order to compensate for this, we nudged all simulations to the wind fields obtained from the simulation FREE_WIND.

Various studies have shown that nudging can affect some of the model processes which strongly depend on wind and precipitation levels, like, for instance, cloud formation and dust and sea salt emissions (Astitha et al., 2012; Lin et al., 2016; Sun et al., 2019). This may also affect the ERF values obtained in nudged simulations (Forster et al., 2016). However, in this study the area affected by the changing emissions is quite small and thus the wind fields are not expected to change much, especially on the global scale. In order to minimize the effect the nudging has on the modeled ERF values, we nudged here towards model simulated (simulation FREE_WIND) derivatives of wind field (vorticity and divergence) and surface pressure, and did not nudge the model temperature at all. This has been shown to reduce the effects of nudging (Lin et al., 2016; Sun et al., 2019; Zhang et al., 2014) on ERF. In summary, the ERF values obtained in this study do not include all the possible rapid adjustments (Forster et al., 2016), and thus, do not correspond to the conventional definition of ERF. In order to highlight this difference, we denote here our ERF as $\mathrm{ERF_{NDG}}$.

3 Results

In this section, we examine and compare the obtained changes in atmospheric aerosol concentrations and radiative fluxes separately for specific regions for Chile and Mexico. Finally, we compare the Chilean and Mexican SO_2 emission effects on global ERF to the effects of Chinese anthropogenic SO_2 emissions. Throughout this section, all values presented are averaged over the entire simulation period. Changes in a value are always with respect to the reference simulation (BASE).

3.1 Determining the area for analysis

As the anthropogenic emissions from Chile and Mexico are small compared to the global total, the area that is significantly influenced by these emissions is also relatively small. Consequently, the radiative effects of these emissions are small on a global scale as well. However, their regional impact can still be important. We therefore focus on the areas where the Chilean and Mexican aerosol emissions are most likely to affect radiation both directly and indirectly.

To this end, we constrained our regions of interest (ROI) to the areas with noticeable changes in vertically integrated aerosol and cloud droplet concentrations (burdens). As a measure of changes in aerosol number burden, we calculated the relative differences between the perturbed simulations (NO_BC, NO_OC, and NO_SO2) and the reference simulation (BASE) for aerosol particles that have diameters greater than 100 nm ($\mathrm{N_{100}}$). Similarly, we calculated the differences for cloud droplet number concentration (CDNC) burden. However, the changes in CDNC burden between two simulations show quite large model-internal variation, even though the simulations are nudged.

To improve the signal-to-noise ratio, we applied the Gaussian smoothing algorithm explained in Appendix A to the CDNC burden changes. Finally, we selected the regions where we see a relative decrease higher than 2 % for $\mathrm{N_{100}}$ burden and 1.5 % for Gaussian-filtered CDNC burden when compared to the reference simulation. The percentage thresholds were chosen such that the resulting region had maximum extent while still being continuous. This results in different areas with respect to aerosol and CDNC burden change, which are shown in Figure 1a. These six regions were then combined into one total. To

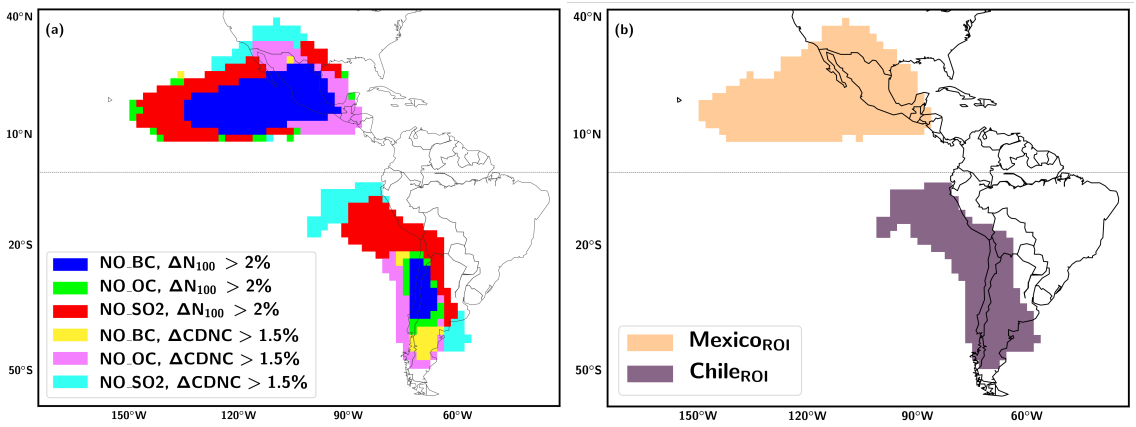

Figure 1. (**a**) The areas where the relative decrease in N_{100} is larger than 2 % (blue, green and red for NO_BC, NO_OC and NO_SO2, respectively) and in CDNC levels larger than 1.5 % (yellow, pink and cyan for NO_BC, NO_OC and NO_SO2, respectively). (**b**) ROIs used for the data analysis, marked for Mexico (orange) and Chile (purple).

Burden ($\mu g\,m^{-2}$)	$Chile_{ROI}$	$Mexico_{ROI}$	Global
NO_BC: BC	-24.3 ± 1.9 $((-4.8 \pm 0.4)\,\%)$	-75.2 ± 3.8 $((-12.2 \pm 0.6)\,\%)$	-6.5 ± 0.6 $((-0.8 \pm 0.1)\,\%)$
NO_OC: OC	-67.2 ± 24.0 $((-2.0 \pm 0.7)\,\%)$	-171.1 ± 13.7 $((-4.8 \pm 0.4)\,\%)$	-16.8 ± 7.2 $((-0.3 \pm 0.1)\,\%)$
NO_SO2: SO_4	-159.5 ± 14.1 $((-3.9 \pm 0.3)\,\%)$	-268.9 ± 19.7 $((-5.7 \pm 0.4)\,\%)$	-28.1 ± 4.4 $((-0.6 \pm 0.1)\,\%)$
MITIG: BC	-10.5 ± 1.5 $((-2.1 \pm 0.3)\,\%)$	-30.3 ± 1.6 $((-4.9 \pm 0.3)\,\%)$	-2.8 ± 0.4 $((-0.3 \pm 0.1)\,\%)$
MITIG: OC	-32.9 ± 16.2 $((-1.0 \pm 0.5)\,\%)$	-71.9 ± 8.5 $((-2.0 \pm 0.2)\,\%)$	-9.9 ± 3.8 $((-0.2 \pm 0.1)\,\%)$

Table 3. Difference in average aerosol mass burdens between the perturbed simulations and the reference simulation (BASE). Relative differences are show in parentheses.

ascertain that the resulting ROI was continuous and connected to the source region, possible smaller, separated regions were removed. The resulting ROIs for Chile and Mexico are shown in Fig. 1b. Unless stated otherwise (e.g. Section 3.4.1), we restrict the following analysis to these two ROIs, which we will refer to as $Mexico_{ROI}$ and $Chile_{ROI}$.

3.2 Atmospheric aerosol concentrations

By examining the differences in aerosol mass burdens for each perturbed simulation, we can estimate how much both countries contribute to the aerosol load over their respective ROIs. In addition to the total mass burden, the horizontal and vertical distribution of the particles, especially with respect to the cloud layer, determines their impacts on the radiative balance. The average differences between the perturbed simulations and the reference simulation (BASE) in aerosol mass burden for BC, OC and SO_4 (averaged over the entire simulation period and the respective ROI area) are shown in Table 3.

Even though we restrict our analysis to $Chile_{ROI}$ and $Mexico_{ROI}$, the changes in BC, OC and SO_4 burdens due to the removal of the anthropogenic emissions of these substances in Chile and Mexico are fairly small. This is mostly due to natural background

emissions and emissions from other countries. Furthermore, in order to obtain ROIs that are as large as possible, we chose very small threshold values, which directly affects the average burden changes in the ROIs. Due to differences in orography, meteorology and horizontal distribution of the emissions in Chile and Mexico, the aerosol particles in $\text{Chile}_{\text{ROI}}$ and $\text{Mexico}_{\text{ROI}}$ are transported differently with in the respective ROIs as well.

The Chilean anthropogenic emissions seem to make a fairly small contribution to the BC and SO_4 burden values over $\text{Chile}_{\text{ROI}}$, and even smaller to the OC burden. For $\text{Chile}_{\text{ROI}}$, we find that the total BC burden decreases by $(4.8 \pm 0.4)\,\%$, whereas for OC the decrease is only $(2.0 \pm 0.7)\,\%$. The SO_4 burden also decreases $(3.9 \pm 0.3)\,\%$. For scenario MITIG, the decrease in the BC and OC burdens is in line with the emission reductions: the decrease in BC burden is almost half of the decrease observed for NO_BC simulation, and similarly for OC burden.

As for Chile, the emissions from Mexico make a rather small contribution on the SO_4 and OC burden over $\text{Mexico}_{\text{ROI}}$. The burden changes over $\text{Mexico}_{\text{ROI}}$ are, however, larger than over $\text{Chile}_{\text{ROI}}$ in both absolute and relative terms (see Table 3). With $(-75.2 \pm 3.8)\,\mu\text{g}\,\text{m}^{-2}$, which corresponds to $(-12.2 \pm 0.6)\,\%$, the decrease in BC burden over $\text{Mexico}_{\text{ROI}}$ is substantial.

As in the scenario MITIG BC and OC emissions are reduced by 50 % and 40 %, respectively, one could expect that the BC and OC burdens in MITIG would decrease by similar percentages of the NO_BC and NO_OC scenarios, if the burdens depended linearly on the emissions. For the OC burden change this holds true, but the BC burden only decreases by 40 % compared to the burden change for the NO_BC simulation. This can be explained by a decrease in hygroscopicity of the emitted BC-containing aerosol, which makes them less susceptible to wet deposition.

All in all, it appears that the relative changes in average burden values are slightly larger for $\text{Mexico}_{\text{ROI}}$ than for $\text{Chile}_{\text{ROI}}$. One explanation for this is the differences in spatial distribution of anthropogenic aerosol emissions: Huneeus et al. (2006) state that the main Chilean SO_2 emitters (i.e. copper smelters) are located in the northern part of Chile, from where the emitted sulfate is transported north and northwest and mainly remains at altitudes below 4 km. The sources for BC and OC are mostly in the middle, near the capital region. This causes that the changes in N_{100} are also more spread towards both north and south, resulting in relatively larger ROI for Chile, as shown in Figure 1. In Mexico, the emission sources are also distributed differently along the country for sulfur and BC, but they are not as distinct as for Chile, and all of the emissions are distributed more evenly across the ROI. In addition, because of the geographic location of Chile and Mexico, the contribution to the aerosol mass burdens from other countries may be larger over $\text{Chile}_{\text{ROI}}$ than over $\text{Mexico}_{\text{ROI}}$.

We analyzed also the atmospheric concentrations at different altitudes (not shown). One remarkable difference between $\text{Chile}_{\text{ROI}}$ and $\text{Mexico}_{\text{ROI}}$ is that for BC, OC and SO_4 in $\text{Chile}_{\text{ROI}}$ the concentration changes are highest at the surface and decrease monotonically with altitude. In $\text{Mexico}_{\text{ROI}}$, on the other hand, these profiles show a second local maximum at about 800 hPa. This may be due to many different influences, including the very different orographic profiles of the two ROIs, the altitude of the emission sites and differences in vertical mixing.

3.3 Aerosols and clouds

As indicated in Section 1, one of the motivations for this study was to analyze the effects of anthropogenic aerosol emissions on the maritime stratocumulus (Sc) deck at the Chilean coastline. However, the current configuration for ECHAM-HAMMOZ does not provide output diagnostics for determining different cloud types directly. Hence, we examined the vertical profiles of the annual mean water cloud fraction, using the data

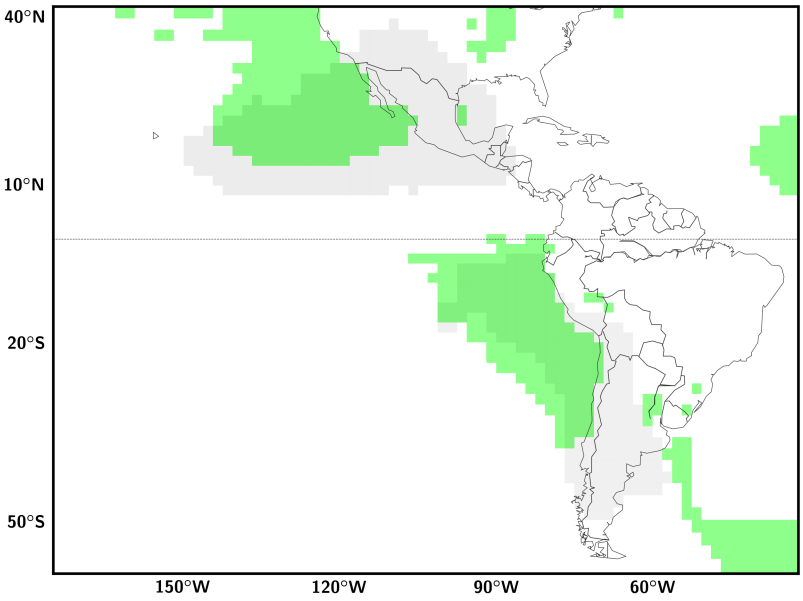

Figure 2. The horizontal distribution of Sc clouds (green) and ROIs (light grey).

from the reference simulation (BASE). Since typical maritime Sc clouds have cloud bases below 2 km and a cloud thickness of less than 1 km (Wood, 2012), we identified grid boxes where the maximum annual mean water cloud fraction was below 900 hPa, and determined those as the areas which are dominated by maritime Sc clouds in our model. These grid boxes are marked in Figure 2, which also shows how much the defined ROIs coincide with these Sc cloud decks.

Besides horizontal distribution, the vertical distribution of aerosol particles and clouds affects the radiative properties. For instance, aerosol particles above cloud layer receive a higher portion of shortwave radiation than below clouds since clouds are efficient on reflecting shortwave (SW) fluxes. This is important for absorbing aerosol, like BC, whose warming effect is often enhanced on top of a cloud (Khn et al., 2014; Zarzycki & Bond, 2010). Because of the differences in local conditions (e.g. atmospheric circulation) for $\text{Chile}_{\text{ROI}}$ and $\text{Mexico}_{\text{ROI}}$, the vertical distributions for aerosol compounds and clouds are studied separately for the two ROIs.

3.3.1 $\text{Chile}_{\text{ROI}}$

For the Chilean anthropogenic emissions, the total mass of SO_2 emitted yearly is remarkably larger than the mass of BC or OC. This can be seen as a high contribution to atmospheric aerosol number concentrations, which further affects the CDNC. The number of particles with diameters larger than 100 nm (N_{100}) is typically considered a proxy for particles that can potentially act as cloud condensation nuclei (CCN) (Dusek et al., 2006; Janssen et al., 2011; Trstl et al., 2016). The vertical concentration difference profiles between perturbed and reference simulation (BASE) for BC mass, N_{100} and cloud droplet number concentration (CDNC) for $\text{Chile}_{\text{ROI}}$ are presented in Figure 3. In order to illustrate the changes in aerosol concentrations with respect to the water cloud layer, we also show the annual average CDNC from the reference simulation (BASE) in each panel. In the model, the altitude of the water clouds follows the CDNC values fairly well.

The vertical location of the atmospheric BC aerosol particles, especially with respect to the clouds, strongly affects BC radiative forcings. Figure 3a shows that most

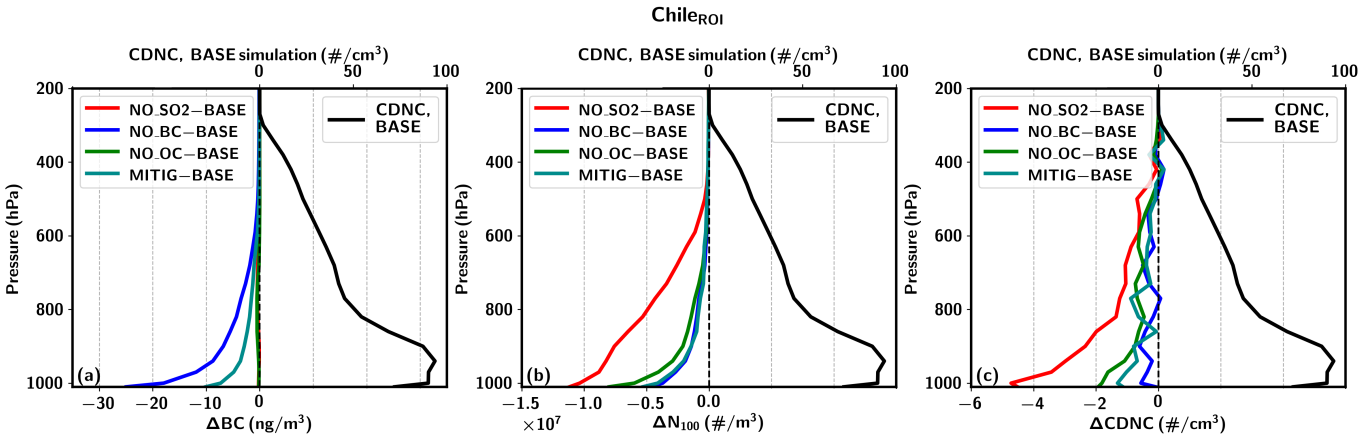

Figure 3. Vertical concentration profiles for (**a**) BC, (**b**) N_{100} and (**c**) CDNC for $Chile_{ROI}$. The differences between perturbed simulations and the reference simulation (BASE) are marked with colored lines (lower x-axis), and the CDNC concentration for the BASE simulation is marked with a black line (upper x-axis).

of the changes in BC concentration are at or below cloud level. As most of $Chile_{ROI}$ is covered with a persistent Sc deck, it can thus be expected that the BC radiative effects are screened by these clouds.

Figure 3b shows the changes in N_{100} for the different scenarios. The sulfur emissions clearly have the strongest effect on N_{100}. Furthermore, due to its high hygroscopicity, sulfur-induced N_{100} changes affect CDNC more than similar changes due to BC and OC. Furthermore, the vertical concentration difference profile of N_{100} for NO_SO2 decreases almost linearly with altitude, while in the other scenarios the decrease is much more rapid. It can therefore be expected that sulfate can still affect clouds effectively at much higher altitudes than BC and OC.

As the amount of anthropogenic aerosol emissions decreases, the CDNC decreases as well. Correspondingly, the mean effective radius of cloud droplets increases when the aerosol burden is decreased (not shown). However, the maximum difference in the effective radius can be observed at 970 hPa with less than 0.1 µm ((0.7 ± 0.3) %) increase for the NO_SO2 simulation, which is a relatively small change. Here the decreasing aerosol number burden reduces the number of cloud droplets, and thus the water is distributed to a smaller amount of particles. This indicates that the clouds appear less bright when there are fewer aerosol particles, and thereby the clouds scatter less radiation (Twomey, 1977). We will show later in Section 3.4 that the indirect forcing is remarkably stronger than direct aerosol forcing for $Chile_{ROI}$.

Since the aerosol emission reductions lead to larger cloud droplets, the remaining droplets precipitate more easily due to higher mass. This can be observed as decreasing mean cloud water content (not shown). However, this decrease is relatively small and is accompanied by a large uncertainty. Taken together with the ongoing discussion of how well this second indirect effect (Albrecht, 1989) is represented in climate models (Malavelle et al., 2017; Mülmenstädt & Feingold, 2018), we will here not analyze this effect further.

3.3.2 Mexico$_{ROI}$

The vertical concentration difference profiles between perturbed and reference simulation (BASE) for BC, N_{100} and CDNC for $Mexico_{ROI}$ are presented in Figure 4. Sim-

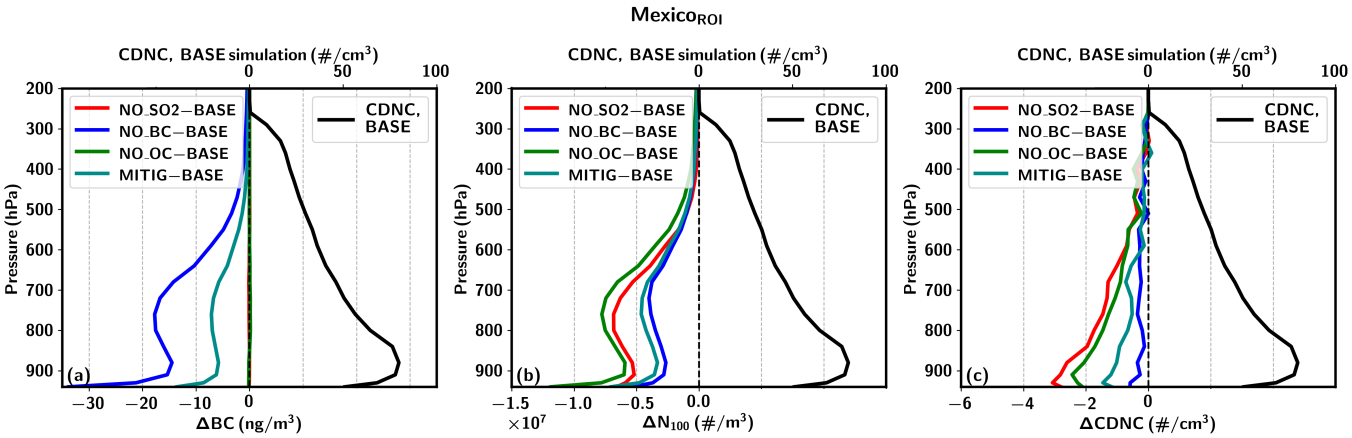

Figure 4. Vertical concentration profiles for (**a**) BC, (**b**) N_{100} and (**c**) CDNC for Mexico$_{ROI}$. The differences between perturbed simulations and the reference simulation (BASE) are marked with colored lines (lower x-axis), and the CDNC concentration for the BASE simulation is marked with a black line (upper x-axis).

ilarly as for Chile$_{ROI}$, the annual mean CDNC concentrations for the BASE simulation are included in all of the panels. As can be seen from Figures 3 and 4, the height of the cloud layer and vertical aerosol concentration profiles are different for Mexico$_{ROI}$ and Chile$_{ROI}$.

In contrast to Chile$_{ROI}$, the changes in BC concentration have a second maximum at the altitude of approximately 750 hPa, which is well above the maximum CDNC of the liquid cloud layer. As BC light absorption is enhanced above clouds, this can be expected to lead to a difference in radiative forcings between Chile$_{ROI}$ and Mexico$_{ROI}$. The vertical profiles for OC and SO_4 (not shown) have a second maximum at about 750 hPa as well.

While in Chile$_{ROI}$ the SO_2 emissions affect N_{100} most, the OC emissions from Mexico affect the N_{100} levels more than SO_2. However, sulfur emissions have a stronger effect on CDNC than BC and OC emissions, even though the effect is not as noticeable as for Chile$_{ROI}$. Since the hygroscopicity of OC is lower than that of sulfur, the OC particles do not form cloud droplets as effectively as SO_4. That is why the differences in N_{100} levels do not directly correspond to the differences observed for CDNC, and thus the Mexican sulfur emissions affect the CDNC values more. The changes for cloud droplet radius are of the same order of magnitude as for Chile$_{ROI}$, including high uncertainty (not shown).

The vertical concentration profiles for Chile$_{ROI}$ and Mexico$_{ROI}$ differ because of the differences in the ROIs (e.g. total area, spatial distribution of emissions), and also due to the differences in atmospheric circulation patterns, solar insolation, precipitation levels and aerosol transport. Furthermore, a large part of the Mexican aerosol emissions are released at rather high altitudes, e.g. since one of the major source regions, Mexico City, is located at 2200 m.

3.4 Radiative forcing

The differences in the aerosol mass burdens and the vertical concentration profiles between Chile$_{ROI}$ and Mexico$_{ROI}$ ultimately also lead to different radiative forcings for the two ROIs. Figure 5 shows the aerosol direct radiative forcing (RF_A) and the ERF_{NDG}

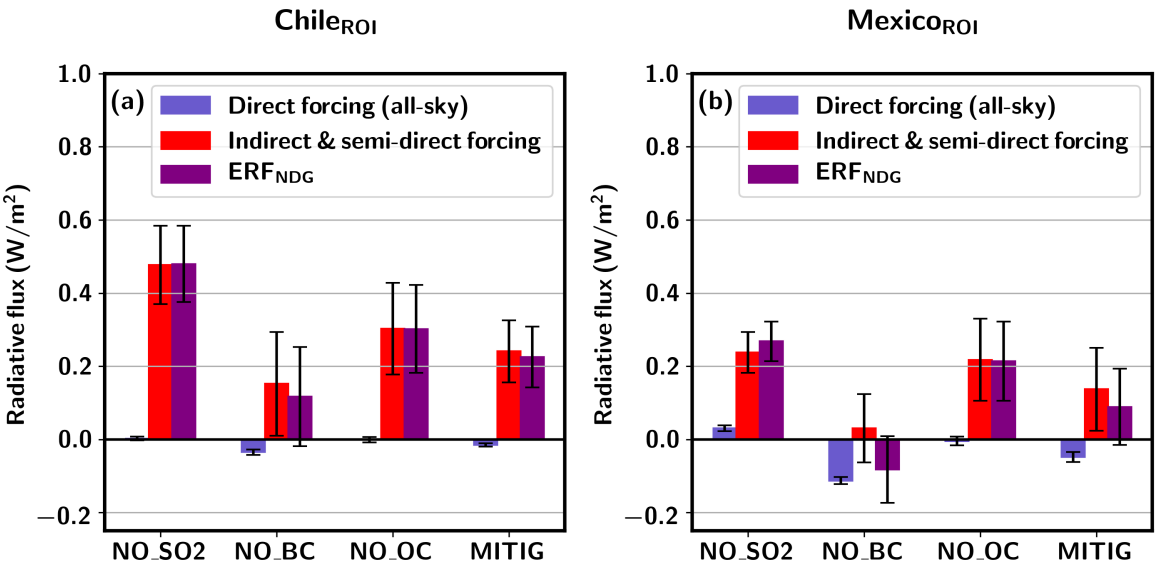

Figure 5. RF_A and ERF_{NDG} for (**a**) $Chile_{ROI}$ and (**b**) $Mexico_{ROI}$.

	RF_A (W m^{-2})		ERF_{NDG} (W m^{-2})	
simulation	$Chile_{ROI}$	$Mexico_{ROI}$	$Chile_{ROI}$	$Mexico_{ROI}$
NO_SO2	0.002 ± 0.005	0.030 ± 0.008	0.480 ± 0.105	0.268 ± 0.054
NO_BC	-0.035 ± 0.008	-0.113 ± 0.010	0.117 ± 0.136	-0.082 ± 0.091
NO_OC	-0.001 ± 0.007	-0.004 ± 0.012	0.302 ± 0.120	0.213 ± 0.108
MITIG	-0.015 ± 0.005	-0.048 ± 0.013	0.225 ± 0.083	0.089 ± 0.104
0.5*NO_BC+0.4*NO_OC	-0.018 ± 0.007	-0.058 ± 0.009	0.179 ± 0.116	0.044 ± 0.089

Table 4. The mean direct all-sky aerosol forcing (RF_A) and ERF_{NDG} at the TOA for $Chile_{ROI}$ and $Mexico_{ROI}$.

for the perturbed simulations. In order to distinguish the aerosol indirect and semi-direct effects, we visualize separately the difference between ERF_{NDG} and RF_A. The numerical values of Figure 5 are presented in Table 4. For all simulations, the 2D ERF_{NDG} signal due to the emission perturbations is well covered by the ROIs defined in Section 3.1 (see Figure B1).

As shown earlier in Figures 1 and 2, the sulfate particles from Chile are mostly transported to the maritime stratocumulus region. This explains what we can observe from Figure 5: the RF_A for NO_SO2 simulation is only slightly positive for $Chile_{ROI}$, while the ERF_{NDG} is the largest in all scenarios and both ROIs. In this region, the RF_A for sulfate is screened by the clouds, but the cloud effects, especially the Twomey effect, are strong. As BC is a strong absorber, the removal of anthropogenic BC in the NO_BC simulation produces a negative RF_A. Yet, as discussed in Section 3.3, the anthropogenic BC emissions affect atmospheric BC concentrations mostly inside or below clouds. That is why the all-sky BC RF_A is fairly small for $Chile_{ROI}$. Similarly as for the Chilean sulfur emissions, the RF_A for OC is negligible ((-0.001 ± 0.007) W m^{-2}). Although the area where we can observe the largest decreases of OC burden is outside of the stratocumulus deck at the Chilean coast (Figure 2), most of the OC aerosol is masked by higher-level clouds.

The ERF_{NDG} values for $Chile_{ROI}$ are positive for all the perturbed simulations, but include wider uncertainty ranges than the corresponding RF_A values. As observed in Section 3.3, the changes in CDNC levels are highest for NO_SO2, which translates to a large ERF_{NDG}, with local maximum values of about $3\,W\,m^{-2}$ (see Figure B1). The ERF_{NDG} signal for NO_OC is also positive ($(0.3 \pm 0.1)\,W\,m^{-2}$), as the changes in CDNC close to the surface are the second largest of all scenarios (see Figure 3). The ERF_{NDG} for the NO_BC simulation, on the other hand, is the smallest of all scenarios, which is due to the negative RF_A and much smaller changes in CDNC levels.

For $Mexico_{ROI}$, the RF_A for the NO_SO2 simulation is only slightly positive, and like for $Chile_{ROI}$, for OC the RF_A is negligible. In contrast to NO_OC and NO_SO2, the RF_A for NO_BC is considerably negative, i.e. removing BC induces cooling of the atmosphere when analyzing only the direct effects. In general, the direct BC forcing is known to be more efficient when BC particles are located above highly reflecting surfaces, such as clouds, which is in contrast to dark, absorbing surfaces such as oceans. As discussed in Section 3.3, the portion of BC emitted from Mexico that ends up above cloud is considerably larger than that emitted from Chile (Figures 3 and 4), which can partly explain why the direct BC RF_A is larger for $Mexico_{ROI}$ than for $Chile_{ROI}$. In addition, the changes in BC burden in $Mexico_{ROI}$ are approximately three time higher than in $Chile_{ROI}$, which suggests a rather linear relation between BC burden and RF_A. While in $Chile_{ROI}$ removing of BC (NO_BC) causes positive ERF_{NDG} values, the ERF_{NDG} values for removing BC in $Mexico_{ROI}$ are negative ($(-0.08 \pm 0.09)\,W\,m^{-2}$). This is because here the RF_A is much stronger and the indirect and semi-direct effects are smaller than in $Chile_{ROI}$. However, the standard deviation is noteworthy. For NO_SO2, the ERF_{NDG} is positive with the value of $(0.27 \pm 0.05)\,W\,m^{-2}$, and the variance is smaller than for NO_BC. As for $Chile_{ROI}$, over $Mexico_{ROI}$ the indirect and semi-direct effects are dominating for NO_OC, with positive ERF_{NDG} values of $(0.2 \pm 0.1)\,W\,m^{-2}$.

The radiative effects for $Chile_{ROI}$ and $Mexico_{ROI}$ differ partly due to unequal ROIs: the ROI defined for Mexico covers relatively more ocean than $Chile_{ROI}$, which causes the mean surface albedo of $Mexico_{ROI}$ to be smaller than for $Chile_{ROI}$. In addition, $Chile_{ROI}$ is in general cloudier than $Mexico_{ROI}$. Clouds mask some of the incoming SW radiation (cloud screening effect), reducing the solar radiation reaching the aerosol particles. This results in smaller RF_A values for $Chile_{ROI}$ compared to $Mexico_{ROI}$. Inversely, aerosol-cloud interactions are stronger for $Chile_{ROI}$ than for $Mexico_{ROI}$, evident through the higher ERF_{NDG} values for $Chile_{ROI}$ compared to $Mexico_{ROI}$. This can to the largest part be explained with the existence of the maritime Sc deck west and northwest of Chile, which is very susceptible to changes in aerosol concentrations. Furthermore, $Chile_{ROI}$ has a relatively larger extent, with sulfur emissions mostly in the northern part of the country, and BC and OC emissions in the middle. This causes the sulfate particles to be transported north, while BC and OC move more towards the east. In Mexico, the aerosol species are transported mainly to the same direction.

As in MITIG both BC and OC emissions are reduced simultaneously (50 % and 40 %, respectively), it is to be expected that the radiative forcing values somehow reflect the radiative forcing values of both the NO_BC and NO_OC simulations. The RF_A values in MITIG are, to the accuracy of one standard deviation, linear combinations of the RF_A values of NO_BC and NO_OC (see Table 4). However, the obtained ERF_{NDG} values in MITIG cannot be approximated in the same fashion. Using the relation $0.5ERF_{NDG,NO\_BC} + 0.4EF_{NDG,NO\_OC}$, one would obtain 0.179 ± 0.116 and $(0.044 \pm 0.089)\,W\,m^{-2}$ for $Chile_{ROI}$ and $Mexico_{ROI}$, respectively. Since the ERF_{NDG} for NO_OC is positive and much greater than for the NO_BC simulation, the overall ERF_{NDG} for the MITIG simulation is also positive for both $Chile_{ROI}$ and $Mexico_{ROI}$, despite the negative ERF_{NDG} obtained for NO_BC in $Mexico_{ROI}$. This demonstrates the complex interplay between aerosol-radiation and aerosol-cloud effects of different, co-emitted aerosol species, which has also been reported in other studies (W.-T. Chen et al., 2010; Huang et al., 2018; Wang et al., 2015).

Like in Huang et al. (2018) and Khn et al. (2020), our results underline the importance of including the reductions of co-emitted species when analysing the effects of BC mitigation.

One remarkable feature is the dominant contribution of the indirect and semi-direct effects to the ERF_{NDG} in $Chile_{ROI}$ due to BC. On the other hand, the indirect BC forcing was small for $Mexico_{ROI}$. This is most likely due to the combination of various processes, e.g. smaller Twomey effect, more BC above cloud and BC-induced changes in the heat balance of the cloud layer.

Even though the simulations in this study where nudged in order to minimize model-internal variation, the ERF_{NDG} standard deviations are still quite notable. This might be partly due to the rather small analyzed area, and the fact that the anthropogenic aerosol emissions of Chile and Mexico are quite small compared to the sum of all natural and anthropogenic sources affecting $Chile_{ROI}$ and $Mexico_{ROI}$. Of all variables analyzed, the changes in cloud properties showed the largest standard deviations. Determining individual processes that affect the radiation indirectly in ECHAM-HAMMOZ is difficult and therefore out of the scope of this study.

In addition to clouds, mineral dust emissions in ECHAM-HAMMOZ show great variation (Kokkola et al., 2018). As dust particles act as condensation sink for sulfate, an increase in mineral dust emissions might lead to less new particle formation for sulfur (Neubauer et al., 2019). Therefore, in addition to the direct effects of dust emissions, the natural variation in background mineral dust might contribute to the high standard deviation observed for ERF_{NDG}.

3.4.1 Impact of the location of emissions reductions

Contrary to the radiative effects of well-mixed greenhouse gases, such as carbon dioxide, aerosol radiative effects show much stronger horizontal variability, mostly due to the much shorter atmospheric lifetime of aerosols (IPCC, 2013). In addition, aerosol particles emitted in the mid-latitudes are likely to induce a different radiative forcing than particles from regions near the equator (Khn et al., 2014; Laakso et al., 2017), because average solar insolation is strongest at the equator. In order to set the ERF_{NDG} for Chilean and Mexican SO_2 emissions into global context, we compare them to the ERF_{NDG} for Chinese anthropogenic SO_2 emissions. For this purpose, we define the global radiative forcing efficiency, EFF_{ERF}, as the ratio between the global ERF_{NDG} (i.e. averaged over the entire globe) and the total emission reduction in a country. The global ERF_{NDG} and calculated EFF_{ERF} values for NO_SO2 and NO_SO2_china simulations are presented in Table 5.

Apart from China being located further away from the equator, the Chinese aerosol-cloud interactions are presumably more saturated (Khn et al., 2014) due to much higher aerosol burdens there. This means that the emission reductions from China are expected to be less efficient than from countries where the aerosol emissions are smaller. This is also the case when analyzing the simulation data. SO_2 reductions from Chile and Mexico show a 20 times higher EFF_{ERF} compared to reductions in China.

However, the global mean ERF_{NDG} for Chile and Mexico has a relatively high standard deviation compared to the actual value ($(0.027 \pm 0.021)\,\mathrm{W\,m^{-2}}$), whereas for emission reductions in China we observe a more robust signal of ($(0.124 \pm 0.023)\,\mathrm{W\,m^{-2}}$). Nevertheless, the obtained results underline the point that the location of aerosol emission mitigation matters when analyzing the global radiative balance.

Simulation	Global ERF_{NDG} ($W\,m^{-2}$)	SO_2 reduction ($kt\,yr^{-1}$)	Efficiency ($W/m^2/(kt/yr)$)
NO_SO2	0.027 ± 0.021	873.67	3.086×10^{-5}
NO_SO2_china	0.124 ± 0.023	15 018.67	0.154×10^{-5}

Table 5. Global mean ERF_{NDG} for NO_SO2 and NO_SO2_china simulations and the emission reductions. The efficiency is defined as a ratio of global ERF_{NDG} and total SO_2 emission reduction.

4 Discussion and Conclusions

The purpose of this study was to demonstrate how emission mitigation in different countries and regions can have diverse, and even contrasting potential to affect the atmospheric radiative balance. The motivation for this study stems from the current discussion on the potential of short-lived climate forcer (SLFC) mitigation to slow down global warming. We focused on analyzing the climatic effects of anthropogenic black carbon (BC), organic carbon (OC) and sulfur dioxide (SO_2) originating from Chile and Mexico. These two Latin American countries have released ambitious climate programs that also consider SLCF emissions, including even specified reduction levels for their BC emissions. In addition, the Chilean local climate is strongly influenced by a persistent stratocumulus cloud deck west of Chile, which makes it an interesting target for studying aerosol-cloud interactions with large scale climate models. A similar, but less persistent cloud deck also exists west and northwest of Mexico.

For distinguishing the effects of different aerosol species, we compared a reference simulation with all aerosol species present (BASE) against perturbed cases without anthropogenic emissions of BC, OC and SO_2 originating from Chile and Mexico (NO_BC,NO_OC and NO_SO2, respectively). Furthermore, in order to study the effect of co-emitted species of BC, we performed one further simulation (MITIG) with Mexican and Chilean anthropogenic BC and OC emissions reduced by 50 % and 40 %, respectively. The results were then analyzed for specific regions of interest ($Chile_{ROI}$ and $Mexico_{ROI}$), defined for the areas where we could observe notable changes in the aerosol and cloud properties. As these ROIs were relatively small, we nudged the wind and surface pressure in all simulations to the same values.

For both $Chile_{ROI}$ and $Mexico_{ROI}$, the obtained indirect and semi-direct aerosol radiative forcings were much stronger than the direct forcings. When removing BC, which strongly absorbs solar radiation, we obtained negative direct radiative forcing, RF_A. Eliminating anthropogenic sulfur emissions resulted in small positive direct forcing, since the sulfur particles are known to back-scatter incoming solar radiation. However, the magnitude of this effect was much smaller than for BC. For OC, the RF_A was virtually negligible.

In order to study aerosol-cloud effects for the perturbed simulations, we calculated the effective radiative forcing (ERF), which includes direct, semi-direct and indirect effects. As our simulations where nudged, however, the simulations do not consider some climate feedbacks. For NO_SO2 and NO_OC, ERF was positive for both $Chile_{ROI}$ and $Mexico_{ROI}$, as expected, dominated by the indirect and semi-direct effects. The NO_BC case is more interesting, however, as the magnitudes of the direct and indirect effects are roughly of the same order but opposite in sign. This resulted in a positive ERF for $Chile_{ROI}$ and a negative ERF for $Mexico_{ROI}$, both values also having an uncertainty that is roughly of similar magnitude as the estimate itself. This result highlights the difficulty in antic-

ipating the ERF caused by reducing BC emissions without simulating the effects of mitigation.

Due to different characteristics of the local climates and especially cloud layers, the ERF signals differ between $\text{Chile}_{\text{ROI}}$ and $\text{Mexico}_{\text{ROI}}$. These features include, for instance, local cloud cover, land orography and background aerosol profile. As the cloud layer near the Chilean coast is thicker than the cloud layer west of Mexico, the direct forcings for the reflecting aerosol are smaller for $\text{Chile}_{\text{ROI}}$ than $\text{Mexico}_{\text{ROI}}$. This is due to the cloud screening effect, where aerosol below cloud receives much less radiation, and because the the radiative effect of reflecting aerosol above a reflecting surface is strongly reduced. Furthermore, the average solar insolation is stronger near the equator, which can contribute to the differing ERF values for these two ROIs. One explanation for differing ERF values is that in Chile the anthropogenic SO_2 emissions are more pronounced when comparing to BC and OC than in Mexico. In addition, a large portion of the anthropogenic aerosol particles in $\text{Mexico}_{\text{ROI}}$ are transported to altitudes above the cloud layer, making the BC RF_A more pronounced for $\text{Mexico}_{\text{ROI}}$. Previous studies have shown that low-level clouds are generally poorly represented by atmospheric general circulation models (Klein et al., 2013). It has to be noted that like many global climate models, ECHAM-HAMMOZ underestimates the persistent stratocumulus deck west of Chile (Stevens et al., 2013). It is therefore to be expected that the ERF values found here would be stronger if the Sc decks west of Chile and Mexico were simulated more realistically.

For the MITIG simulation, the estimated ERF was positive for both $\text{Chile}_{\text{ROI}}$ and $\text{Mexico}_{\text{ROI}}$. This demonstrates that the indirect and semi-direct effects due to BC and OC removal counter-act the negative direct forcing caused by reduced BC emissions, leading to an overall warming effect. The reduction in emission strength of BC and OC in the MITIG scenario was based on simplified assumptions and the ERF values obtained here would probably change if a more realistic scenario was used.

Since one of our aims was to investigate how much emission location affects the obtained results, we performed another simulation where we removed all anthropogenic SO_2 emissions from China. We found that the anthropogenic SO_2 emissions from Chile and Mexico induce an almost 20 times higher ERF per emitted unit mass than the SO_2 emissions from China. We concluded that the main cause of this difference is the non-linearity of aerosol-cloud interactions, which leads to a saturation of these effects over China, where anthropogenic emission strengths are amongst the highest of the world. Other causes include different insolation levels and differences in local meteorology.

In this study all simulations were nudged towards the same wind and surface pressure fields. This helped to greatly reduce model-internal variability and thereby uncertainty intervals when comparing to similar studies without nudging (Baker et al., 2015; Cherian et al., 2017; Khn et al., 2020). However, the uncertainty intervals obtained for the ERF values still were of the order of the ERF values themselves. This is partly due to the small area affected by the emissions studied here and partly due to further model-internal variability which cannot be suppressed through nudging. A trade-off for the reduced uncertainty intervals due to nudging is the suppression of some feedback mechanisms in the model. Simulations with free meteorology or even fully coupled Earth system models may therefore find different values for the effective radiative forcings calculated here (Forster et al., 2016). Furthermore, TOA radiative forcing may not be the optimal measure for analyzing the warming potential of BC, as the vertical and spatial placement of BC particles determines whether the overall effect is warming or even cooling (Flanner, 2013; Yang et al., 2019).

The results obtained in this study underline how the changes in radiative balance due to aerosol mitigation are not linearly dependent on the total aerosol mass emitted. In other words, at some locations aerosol mitigation can reduce local warming or cooling effects more efficiently than in other regions, even if the emissions are relatively small.

Besides climatic effects, SLCF mitigation could lead to improved surface air quality and thereby reduce negative health effects of these harmful pollutants. Thus, this may encourage also countries with fairly small yearly emissions to include SLCF mitigation in their climate and air quality efforts. In addition, limiting the region of analysis to areas with notable changes in aerosol and cloud properties provided a good platform to study the ERF for anthropogenic aerosol, and thus could be used to evaluate the effects of SLCF mitigation for other countries as well.

Appendix A Gaussian smoothing

Several of the quantities analysed in this study show considerable variability both in space and time, even though the simulations where nudged towards the same wind and surface pressure fields. This makes it hard to detect signals, especially when looking at 2D maps. However, often the modeled variability is correlated: if in one grid box a value is higher than the areal average, it will be lower in another nearby grid box. In order to to be able to distinguish between actual signals (differences between two simulations) and especially large outliers, we smoothed some of the 2D data using a Gaussian filter. Using the grid indices i, i', j, and j', we define the Gaussian Kernel as

$$G_{ii'jj'} = \exp\left(-\frac{(i-i')^2 + (j-j')^2}{\sigma^2}\right) \tag{A1}$$

The smoothed data, $\widetilde{F}_{ij}$, is then calculated from the raw data, F_{ij}, as

$$\widetilde{F}_{i'j'} = \frac{\sum_{i',j'} F_{ij} G_{ii'jj'}}{\sum_{i'j'} G_{ii'jj'}} \tag{A2}$$

For computational efficiency we only performed the summation in Eq. A2 for values of $G_{ii'jj'} > 10^{-3}$. For the width σ we used here a value of 2 for smoothing the CDNC burden data in Section 3.1 and a value of 1.5 for smoothing the ERF data in Figure B1. Note that this smoothing technique not only removes noise, but also blurs features of the data. Therefore, in any 2D maps of smoothed data shown (for instance in Figure B1) the actual features may be sharper, but larger in magnitude. The amount of blurring depends on the value used for σ. An example of the effects of this Gaussian filtering is shown in Figure A1

Appendix B The horizontal $\mathbf{ERF_{NDG}}$ distribution

The Gaussian-smoothed spatial distribution of $\mathrm{ERF_{NDG}}$ values for the different emission reduction scenarios in $\mathrm{Chile_{ROI}}$ and $\mathrm{Mexico_{ROI}}$ is presented in Figure B1. The figure demonstrates very well, how different aerosol species affect the $\mathrm{ERF_{NDG}}$ values very differently in terms of both magnitude and horizontal distribution. As can be seen from the figures, the regions where the $\mathrm{ERF_{NDG}}$ is affected by the emission changes is well included in $\mathrm{Chile_{ROI}}$ and $\mathrm{Mexico_{ROI}}$.

Acknowledgments

This work was financially supported by the Academy of Finland Center of Excellence programme (grant no. 307331), Academy of Finland projects no. 308292 and 283031, European Research Council (ERC Starting Grant 678889) and the University of Eastern Finland Doctoral School Program in Environmental Physics, Health and Biology. For computational resources, we acknowledge CSC IT Center for Science, Finland. The ECHAM-HAMMOZ model is developed by a consortium composed of the ETH Zrich, Max Planck Institut fr Meteorologie, Forschungszentrum Jlich, University of Oxford, Finnish Meteorological Institute, and Leibniz Institute for Tropospheric Research, and is managed by the Center for Climate Systems Modeling (C2SM) at ETH Zrich.

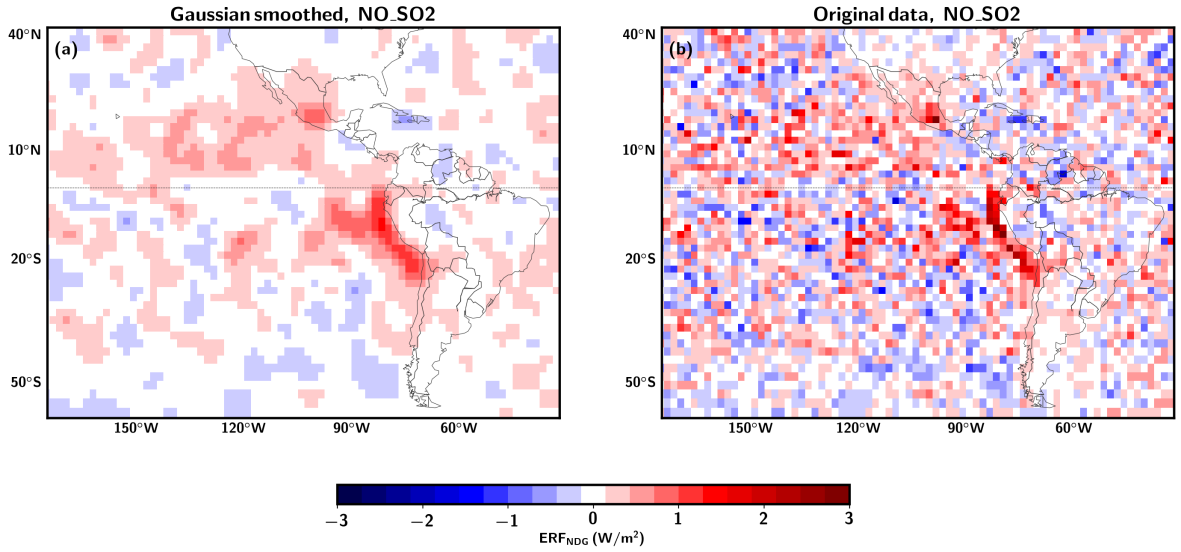

Figure A1. The Gaussian smoothed and original ERF_{NDG} as a 2D visualisation.

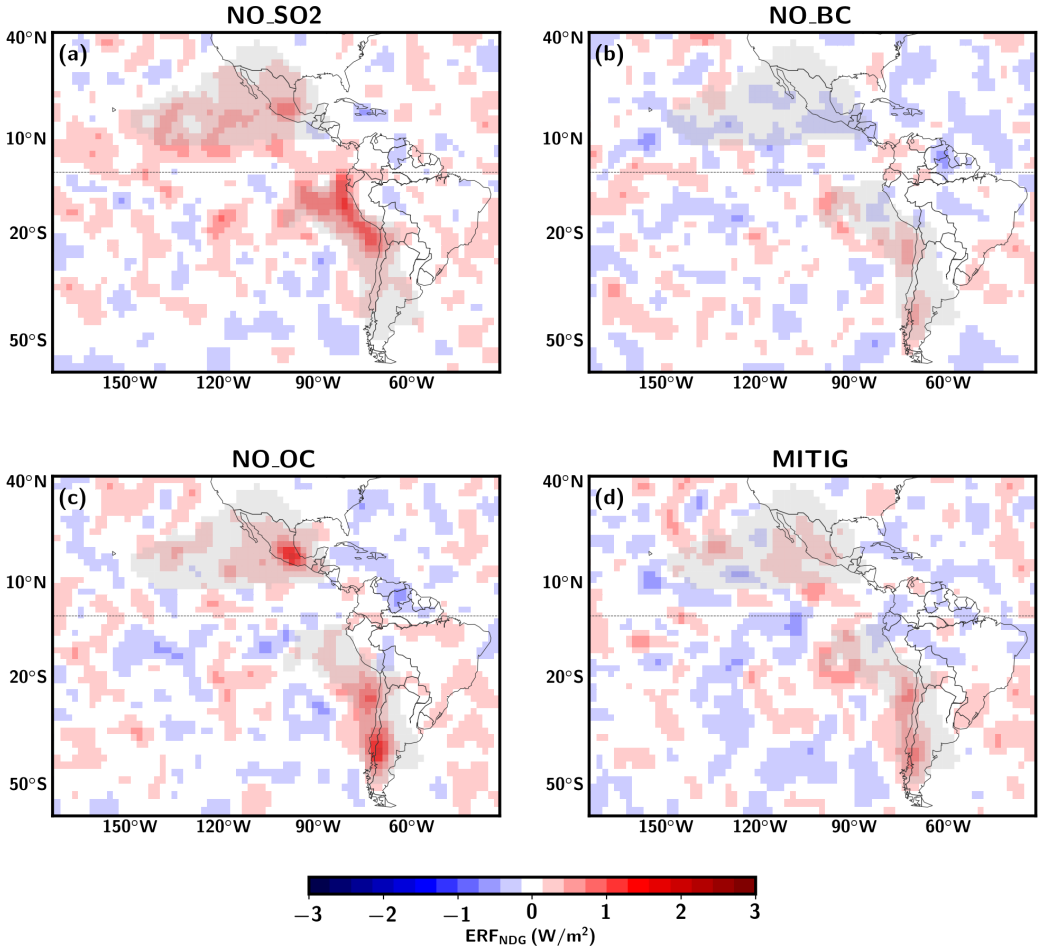

Figure B1. The Gaussian-smoothed spatial distribution of ERF_{NDG} for perturbed simulations. The areas of analysis, $Chile_{ROI}$ and $Mexico_{ROI}$ are indicated in grey in each map.

We acknowledge IIASA institute for providing the ECLIPSE V6a emission input files.

Author contributions. TM wrote the majority of the paper. TM performed all the simulations. TM, TK and HK conducted the data analysis. All authors contributed to the writing process and designing of the study.

Data availability. The model data can be reproduced using ECHAM-HAMMOZ model revision 5914 from the repository https://redmine.hammoz.ethz.ch/projects/hammoz/repository/show/echam6-hammoz/branches/5914 (HAMMOZ consortium, 2019). In addition, the data can be obtained directly from the corresponding author. The settings for the simulation are given in folder https://redmine.hammoz.ethz.ch/projects/hammoz/repository/show/echam6-hammoz/branches/fmi/ClimaSlow/miinalainen_2020_settings. (HAMMOZ consortium, 2020). The ECLIPSE V6a emission input files are available upon request. All other emission input files are ECHAM-HAMMOZ standard and are available from the HAMMOZ repository (see https://redmine.hammoz.ethz.ch/ projects/hammoz, HAMMOZ consortium, 2019).

Competing interests. The authors declare that they have no conflict of interest.

References

Aamaas, B., Berntsen, T. K., Fuglestvedt, J. S., Shine, K. P., & Bellouin, N. (2016). Regional emission metrics for short-lived climate forcers from multiple models. *Atmospheric Chemistry and Physics*, *16*(11), 7451–7468. Retrieved from `https://www.atmos-chem-phys.net/16/7451/2016/` doi: 10.5194/acp-16-7451-2016

Abel, S. J., Walters, D. N., & Allen, G. (2010). Evaluation of stratocumulus cloud prediction in the Met Office forecast model during VOCALS-REx. *Atmospheric Chemistry and Physics*, *10*(21), 10541–10559. Retrieved from `https://www.atmos-chem-phys.net/10/10541/2010/` doi: 10.5194/acp-10-10541-2010

Albrecht, B. A. (1989). Aerosols, cloud microphysics, and fractional cloudiness. *Science*, *245*(4923), 1227–1230. Retrieved from `https://science.sciencemag.org/content/245/4923/1227` doi: 10.1126/science.245.4923.1227

Amann, M., Bertok, I., Borken-Kleefeld, J., Cofala, J., Heyes, C., Hglund-Isaksson, L., ... Winiwarter, W. (2011). Cost-effective control of air quality and greenhouse gases in Europe: Modeling and policy applications. *Environmental Modelling & Software*, *26*(12), 1489 - 1501. Retrieved from `http://www.sciencedirect.com/science/article/pii/S1364815211001733` doi: https://doi.org/10.1016/j.envsoft.2011.07.012

AMAP. (2011). The Impact of Black Carbon on Arctic Climate. By: P.K. Quinn, A. Stohl, A. Arneth,T. Berntsen, J. F. Burkhart, J. Christensen, M. Flanner, K. Kupiainen, H. Lihavainen, M. Shepherd, V. Shevchenko,H. Skov, and V. Vestreng. *AMAP Technical Report No. 4*, 72.

AMAP. (2015). *AMAP Assessment 2015: Black carbon and ozone as Arctic climate forcers* [Book]. Oslo, Norway: Arctic Monitoring and Assessment Programme (AMAP). Retrieved from `https://www.amap.no/documents/doc/amap-assessment-2015-black-carbon-and-ozone-as-arctic-climate-forcers/1299`

Astitha, M., Lelieveld, J., Abdel Kader, M., Pozzer, A., & de Meij, A. (2012). Parameterization of dust emissions in the global atmospheric chemistry-climate model emac: impact of nudging and soil properties. *Atmospheric Chemistry and Physics*, *12*(22), 11057–11083. Retrieved from `https://www.atmos-chem-phys.net/12/11057/2012/` doi: 10.5194/acp-12-11057-2012

Baker, L. H., Collins, W. J., Olivié, D. J. L., Cherian, R., Hodnebrog, Ø., Myhre, G., & Quaas, J. (2015). Climate responses to anthropogenic emissions of short-lived climate pollutants. *Atmospheric Chemistry and Physics*, *15*(14),

8201–8216. doi: 10.5194/acp-15-8201-2015

Ban-Weiss, G. A., Cao, L., Bala, G., & Caldeira, K. (2012, Mar). Dependence of climate forcing and response on the altitude of black carbon aerosols. *Climate Dynamics*, *38*(5-6), 897-911. doi: 10.1007/s00382-011-1052-y

Bellouin, N., Quaas, J., Gryspeerdt, E., Kinne, S., Stier, P., Watson-Parris, D., ... Stevens, B. (2020). Bounding global aerosol radiative forcing of climate change. *Reviews of Geophysics*, *58*(1), e2019RG000660. Retrieved from https://agupubs.onlinelibrary.wiley.com/doi/abs/10.1029/2019RG000660 doi: 10.1029/2019RG000660

Bond, T. C., Doherty, S. J., Fahey, D. W., Forster, P. M., Berntsen, T., DeAngelo, B. J., ... Zender, C. S. (2013). Bounding the role of black carbon in the climate system: A scientific assessment. *Journal of Geophysical Research: Atmospheres*, *118*(11), 5380-5552. Retrieved from https://agupubs.onlinelibrary.wiley.com/doi/abs/10.1002/jgrd.50171 doi: 10.1002/jgrd.50171

Boucher, O., Randall, D., Artaxo, P., Bretherton, C., Feingold, G., Forster, P., ... Zhang, X. (2013). Clouds and aerosols [Book Section]. In T. Stocker et al. (Eds.), *Climate change 2013: The physical science basis. contribution of working group i to the fifth assessment report of the intergovernmental panel on climate change* (p. 571658). Cambridge, United Kingdom and New York, NY, USA: Cambridge University Press. Retrieved from www.climatechange2013.org doi: 10.1017/CBO9781107415324.016

Bowerman, N. H. A., Frame, D. J., Huntingford, C., Lowe, J. A., Smith, S. M., & Allen, M. R. (2013). The role of short-lived climate pollutants in meeting temperature goals. *Nature Climate Change*, *3*(12), 1021-1024. Retrieved from https://doi.org/10.1038/nclimate2034 doi: 10.1038/nclimate2034

Burnett, R., Chen, H., Szyszkowicz, M., Fann, N., Hubbell, B., Pope, C. A., ... Spadaro, J. V. (2018, Sep 18). Global estimates of mortality associated with long-term exposure to outdoor fine particulate matter. *Proceedings of the National Academy of Sciences of the United States of America*, *115*(38), 9592-9597. Retrieved from https://search.proquest.com/docview/2099894631?accountid=11739

CCAC, & UNEP. (2016). *Integrated Assessment of Short-Lived Climate Pollutants for Latin America and the Caribbean: improving air quality while mitigating climate change. Summary for decision makers* (Tech. Rep.). Nairobi, Kenya: United Nations Environment Programme.

Chen, G., Wang, W.-C., & Chen, J.-P. (2015). Aerosolstratocumulusradiation interactions over the southeast pacific. *Journal of the Atmospheric Sciences*, *72*(7), 2612-2621. Retrieved from https://doi.org/10.1175/JAS-D-14-0319.1 doi: 10.1175/JAS-D-14-0319.1

Chen, W.-T., Lee, Y. H., Adams, P. J., Nenes, A., & Seinfeld, J. H. (2010). Will black carbon mitigation dampen aerosol indirect forcing? *Geophysical Research Letters*, *37*(9). Retrieved from https://agupubs.onlinelibrary.wiley.com/doi/abs/10.1029/2010GL042886 doi: 10.1029/2010GL042886

Cherian, R., Quaas, J., Salzmann, M., & Tomassini, L. (2017). Black carbon indirect radiative effects in a climate model. *Tellus B: Chemical and Physical Meteorology*, *69*(1), 1369342. Retrieved from https://doi.org/10.1080/16000889.2017.1369342 doi: 10.1080/16000889.2017.1369342

Chile's Nationally Determined Contribution (NDC), Update 2020. (2020). Retrieved from https://www4.unfccc.int/sites/ndcstaging/PublishedDocuments/Chile\%20First/Chile\%27s_NDC_2020_english.pdf

ClimaSlow. (2017). Retrieved from https://www.uef.fi/web/cceel/climaslow

Collins, W. D., Ramaswamy, V., Schwarzkopf, M. D., Sun, Y., Portmann, R. W., Fu, Q., ... Zhong, W. Y. (2006). Radiative forcing by well-mixed greenhouse gases: Estimates from climate models in the intergovernmental panel

on climate change (ipcc) fourth assessment report (ar4). *Journal of Geophysical Research: Atmospheres*, *111*(D14). Retrieved from https://agupubs.onlinelibrary.wiley.com/doi/abs/10.1029/2005JD006713 doi: 10.1029/2005JD006713

Collins, W. J., Fry, M. M., Yu, H., Fuglestvedt, J. S., Shindell, D. T., & West, J. J. (2013). Global and regional temperature-change potentials for near-term climate forcers. *Atmospheric Chemistry and Physics*, *13*(5), 2471–2485. Retrieved from https://www.atmos-chem-phys.net/13/2471/2013/ doi: 10.5194/acp-13-2471-2013

Cruz-Núñez, X. (2014). An approach to a black carbon emission inventory for Mexico by two methods. *Science of The Total Environment*, *479-480*, 181-188. Retrieved from http://www.sciencedirect.com/science/article/pii/S0048969714000734

Ding, A. J., Huang, X., Nie, W., Sun, J. N., Kerminen, V.-M., Petj, T., ... Fu, C. B. (2016). Enhanced haze pollution by black carbon in megacities in China. *Geophysical Research Letters*, *43*(6), 2873-2879. Retrieved from https://agupubs.onlinelibrary.wiley.com/doi/abs/10.1002/2016GL067745 doi: 10.1002/2016GL067745

Dusek, U., Frank, G. P., Hildebrandt, L., Curtius, J., Schneider, J., Walter, S., ... Andreae, M. O. (2006). Size matters more than chemistry for cloud-nucleating ability of aerosol particles. *Science*, *312*(5778), 1375–1378. Retrieved from https://science.sciencemag.org/content/312/5778/1375 doi: 10.1126/science.1125261

Flanner, M. G. (2013). Arctic climate sensitivity to local black carbon. *Journal of Geophysical Research: Atmospheres*, *118*(4), 1840-1851. doi: 10.1002/jgrd.50176

Forster, P. M., Richardson, T., Maycock, A. C., Smith, C. J., Samset, B. H., Myhre, G., ... Schulz, M. (2016). Recommendations for diagnosing effective radiative forcing from climate models for CMIP6. *Journal of Geophysical Research: Atmospheres*, *121*(20), 12,460-12,475. doi: 10.1002/2016JD025320

Ghan, S. J. (2013). Technical note: Estimating aerosol effects on cloud radiative forcing. *Atmospheric Chemistry and Physics*, *13*(19), 9971–9974. Retrieved from https://www.atmos-chem-phys.net/13/9971/2013/ doi: 10.5194/acp-13-9971-2013

Gómez-Sanabria, A., Hglund-Isaksson, L., Rafaj, P., & Schpp, W. (2018). Carbon in global waste and wastewater flows – its potential as energy source under alternative future waste management regimes. *Advances in Geosciences*, *45*, 105–113. Retrieved from https://www.adv-geosci.net/45/105/2018/ doi: 10.5194/adgeo-45-105-2018

Hansen, J., & Nazarenko, L. (2004). Soot climate forcing via snow and ice albedos. *Proceedings of the National Academy of Sciences*, *101*(2), 423–428. Retrieved from https://www.pnas.org/content/101/2/423 doi: 10.1073/pnas.2237157100

Hartmann, D. L., Ockert-Bell, M. E., & Michelsen, M. L. (1992). The effect of cloud type on earth's energy balance: Global analysis. *Journal of Climate*, *5*(11), 1281-1304. Retrieved from https://doi.org/10.1175/1520-0442(1992)005<1281:TEOCTO>2.0.CO;2 doi: 10.1175/1520-0442(1992)005⟨1281:TEOCTO⟩2.0.CO;2

Huang, Y., Unger, N., Storelvmo, T., Harper, K., Zheng, Y., & Heyes, C. (2018). Global radiative effects of solid fuel cookstove aerosol emissions. *Atmospheric Chemistry and Physics*, *18*(8), 5219–5233. Retrieved from https://www.atmos-chem-phys.net/18/5219/2018/ doi: 10.5194/acp-18-5219-2018

Huneeus, N., Gallardo, L., & Rutllant, J. A. (2006). Offshore transport episodes of anthropogenic sulfur in northern chile: Potential impact on the stratocumulus cloud deck. *Geophysical Research Letters*, *33*(19). Retrieved from https://

agupubs.onlinelibrary.wiley.com/doi/abs/10.1029/2006GL026921 doi: 10.1029/2006GL026921

Inness, A., Baier, F., Benedetti, A., Bouarar, I., Chabrillat, S., Clark, H., ... the MACC team (2013). The MACC reanalysis: an 8 yr data set of atmospheric composition. *Atmospheric Chemistry and Physics*, *13*(8), 4073–4109. Retrieved from https://www.atmos-chem-phys.net/13/4073/2013/ doi: 10.5194/acp-13-4073-2013

IPCC. (2013). *Climate change 2013: The physical science basis. contribution of working group i to the fifth assessment report of the intergovernmental panel on climate change* [Book]. Cambridge, United Kingdom and New York, NY, USA: Cambridge University Press. Retrieved from www.climatechange2013.org doi: 10.1017/CBO9781107415324

Janssen, R. H. H., Ganzeveld, L. N., Kabat, P., Kulmala, M., Nieminen, T., & Roebeling, R. A. (2011). Estimating seasonal variations in cloud droplet number concentration over the boreal forest from satellite observations. *Atmospheric Chemistry and Physics*, *11*(15), 7701–7713. Retrieved from https://www.atmos-chem-phys.net/11/7701/2011/ doi: 10.5194/acp-11-7701-2011

Kaiser, J. W., Heil, A., Andreae, M. O., Benedetti, A., Chubarova, N., Jones, L., ... van der Werf, G. R. (2012). Biomass burning emissions estimated with a global fire assimilation system based on observed fire radiative power. *Biogeosciences*, *9*(1), 527–554. Retrieved from https://www.biogeosciences.net/9/527/2012/ doi: 10.5194/bg-9-527-2012

Klein, S. A., & Hartmann, D. L. (1993). The seasonal cycle of low stratiform clouds. *Journal of Climate*, *6*(8), 1587-1606. Retrieved from https://doi.org/10.1175/1520-0442(1993)006<1587:TSCOLS>2.0.CO;2 doi: 10.1175/1520-0442(1993)006⟨1587:TSCOLS⟩2.0.CO;2

Klein, S. A., Zhang, Y., Zelinka, M. D., Pincus, R., Boyle, J., & Gleckler, P. J. (2013). Are climate model simulations of clouds improving? an evaluation using the ISCCP simulator. *Journal of Geophysical Research: Atmospheres*, *118*(3), 1329-1342. Retrieved from https://agupubs.onlinelibrary.wiley.com/doi/abs/10.1002/jgrd.50141 doi: 10.1002/jgrd.50141

Klimont, Z. (2019). *ECLIPSE V6a.* (Personal communication, based on methodology presented in (Klimont et al., 2017).The BC and OC emissions from waste management sector were updated with the methodology described in (Gómez-Sanabria et al., 2018).)

Klimont, Z., Kupiainen, K., Heyes, C., Purohit, P., Cofala, J., Rafaj, P., ... Schpp, W. (2017). Global anthropogenic emissions of particulate matter including black carbon. *Atmospheric Chemistry and Physics*, *17*(14), 8681–8723. Retrieved from https://www.atmos-chem-phys.net/17/8681/2017/ doi: 10.5194/acp-17-8681-2017

Koch, D., & Del Genio, A. D. (2010). Black carbon semi-direct effects on cloud cover: review and synthesis. *Atmospheric Chemistry and Physics*, *10*(16), 7685–7696. Retrieved from https://www.atmos-chem-phys.net/10/7685/2010/ doi: 10.5194/acp-10-7685-2010

Kokkola, H., Khn, T., Laakso, A., Bergman, T., Lehtinen, K. E. J., Mielonen, T., ... Romakkaniemi, S. (2018). SALSA2.0: The sectional aerosol module of the aerosolchemistryclimate model ECHAM6.3.0-HAM2.3-MOZ1.0. *Geoscientific Model Development*, *11*(9), 3833. Retrieved from https://search.proquest.com/docview/2112010641?accountid=11739

Krzyzanowski, M., Apte, J. S., Bonjour, S. P., Brauer, M., Cohen, A. J., & Prss-Ustun, A. M. (2014). Air pollution in the mega-cities. *Current Environmental Health Reports*, *1*(3), 185-191. Retrieved from https://doi.org/10.1007/s40572-014-0019-7 doi: 10.1007/s40572-014-0019-7

Khn, T., Kupiainen, K., Miinalainen, T., Kokkola, H., Paunu, V.-V., Laakso, A., ... Lehtinen, K. E. J. (2020). Effects of black carbon mitigation on Arctic climate. *Atmospheric Chemistry and Physics*, *20*(9), 5527–5546. Retrieved from https://www.atmos-chem-phys.net/20/5527/2020/ doi: 10.5194/acp-20-5527-2020

Khn, T., Partanen, A.-I., Laakso, A., Lu, Z., Bergman, T., Mikkonen, S., ... Laaksonen, A. (2014). Climate impacts of changing aerosol emissions since 1996. *Geophysical Research Letters*, *41*(13), 4711-4718. Retrieved from https://agupubs.onlinelibrary.wiley.com/doi/abs/10.1002/2014GL060349 doi: 10.1002/2014GL060349

Laakso, A., Korhonen, H., Romakkaniemi, S., & Kokkola, H. (2017). Radiative and climate effects of stratospheric sulfur geoengineering using seasonally varying injection areas. *Atmospheric Chemistry and Physics*, *17*(11), 6957–6974. Retrieved from https://www.atmos-chem-phys.net/17/6957/2017/ doi: 10.5194/acp-17-6957-2017

Lamarque, J.-F., Bond, T. C., Eyring, V., Granier, C., Heil, A., Klimont, Z., ... van Vuuren, D. P. (2010). Historical (1850–2000) gridded anthropogenic and biomass burning emissions of reactive gases and aerosols: methodology and application. *Atmospheric Chemistry and Physics*, *10*(15), 7017–7039. Retrieved from https://www.atmos-chem-phys.net/10/7017/2010/ doi: 10.5194/acp-10-7017-2010

Li, C., McLinden, C., Fioletov, V., Krotkov, N., Carn, S., Joiner, J., ... Dickerson, R. R. (2017, Nov 09). India is overtaking China as the world's largest emitter of anthropogenic sulfur dioxide. *Scientific Reports*, *7*(1), 14304. Retrieved from https://doi.org/10.1038/s41598-017-14639-8 doi: 10.1038/s41598-017-14639-8

Lin, G., Wan, H., Zhang, K., Qian, Y., & Ghan, S. J. (2016). Can nudging be used to quantify model sensitivities in precipitation and cloud forcing? *Journal of Advances in Modeling Earth Systems*, *8*(3), 1073-1091. Retrieved from https://agupubs.onlinelibrary.wiley.com/doi/abs/10.1002/2016MS000659 doi: 10.1002/2016MS000659

Lohmann, U., Rotstayn, L., Storelvmo, T., Jones, A., Menon, S., Quaas, J., ... Ruedy, R. (2010). Total aerosol effect: radiative forcing or radiative flux perturbation? *Atmospheric Chemistry and Physics*, *10*(7), 3235–3246. Retrieved from https://www.atmos-chem-phys.net/10/3235/2010/ doi: 10.5194/acp-10-3235-2010

Malavelle, F. F., Haywood, J. M., Jones, A., Gettelman, A., Clarisse, L., Bauduin, S., ... Thordarson, T. (2017). Strong constraints on aerosol–cloud interactions from volcanic eruptions. *Nature*, *546*(7659), 485–491.

Mena-Carrasco, M., Saide, P., Delgado, R., Hernandez, P., Spak, S., Molina, L., ... Jiang, X. (2014). Regional climate feedbacks in Central Chile and their effect on air quality episodes and meteorology. *Urban Climate*, *10*, 771 - 781. doi: https://doi.org/10.1016/j.uclim.2014.06.006

Molina, L. T., Gallardo, L., Andrade, M., Baumgardner, D., Borbor-Cordova, M., Borquez, R., ... Schwarz, J. P. (2015, 12). Pollution and its impacts on the South American cryosphere. *Earth's Future*, *3*(12), 345-369. Retrieved from https://search-proquest-com.ezproxy.uef.fi:2443/docview/1776644206?accountid=11739

Muhlbauer, A., McCoy, I. L., & Wood, R. (2014). Climatology of stratocumulus cloud morphologies: microphysical properties and radiative effects. *Atmospheric Chemistry and Physics*, *14*(13), 6695–6716. Retrieved from https://www.atmos-chem-phys.net/14/6695/2014/ doi: 10.5194/acp-14-6695-2014

Mülmenstädt, J., & Feingold, G. (2018). The radiative forcing of aerosol–cloud interactions in liquid clouds: wrestling and embracing uncertainty. *Current Climate Change Reports*, *4*(1), 23–40.

Mülmenstädt, J., Gryspeerdt, E., Salzmann, M., Ma, P.-L., Dipu, S., & Quaas, J. (2019). Separating radiative forcing by aerosol–cloud interactions and rapid cloud adjustments in the ECHAM–HAMMOZ aerosol–climate model using the method of partial radiative perturbations. *Atmospheric Chemistry and Physics*, *19*(24), 15415–15429. Retrieved from https://www.atmos-chem-phys.net/19/15415/2019/ doi: 10.5194/acp-19-15415-2019

Neubauer, D., Ferrachat, S., Siegenthaler-Le Drian, C., Stier, P., Partridge, D. G., Tegen, I., ... Lohmann, U. (2019). The global aerosol–climate model ECHAM6.3–HAM2.3 – part 2: Cloud evaluation, aerosol radiative forcing, and climate sensitivity. *Geoscientific Model Development*, *12*(8), 3609–3639. Retrieved from https://www.geosci-model-dev.net/12/3609/2019/ doi: 10.5194/gmd-12-3609-2019

Paulot, F., Paynter, D., Ginoux, P., Naik, V., & Horowitz, L. W. (2018). Changes in the aerosol direct radiative forcing from 2001 to 2015: observational constraints and regional mechanisms. *Atmospheric Chemistry and Physics*, *18*(17), 13265–13281. Retrieved from https://www.atmos-chem-phys.net/18/13265/2018/ doi: 10.5194/acp-18-13265-2018

Roeckner, E., Buml, G., Bonaventura, L., Brokopf, R., Esch, M., Giorgetta, M., ... Tompkins, A. (2003). *The atmospheric general circulation model ECHAM 5. part i: Model description.* (Tech. Rep. No. 349). Max-Planck-Institute for Meteorology.

Sand, M., Berntsen, T., von Salzen, K., Flanner, M. G., Langer, J., & Victor, D. G. (2016). Arctic temperature to changes in emissions of short-lived climate forcers. *Nature Clim Change*, *6*(3), 286289.

Sand, M., Berntsen, T. K., Kay, J. E., Lamarque, J. F., Seland, Ø., & Kirkevg, A. (2013). The Arctic response to remote and local forcing of black carbon. *Atmospheric Chemistry and Physics*, *13*(1), 211. Retrieved from https://search.proquest.com/docview/1270759219?accountid=11739

Schultz, M. G., Stadtler, S., Schröder, S., Taraborrelli, D., Franco, B., Krefting, J., ... Wespes, C. (2018). The chemistry–climate model ECHAM6.3-HAM2.3-MOZ1.0. *Geoscientific Model Development*, *11*(5), 1695–1723. Retrieved from https://www.geosci-model-dev.net/11/1695/2018/ doi: 10.5194/gmd-11-1695-2018

SEMARNAT, & INECC. (2016). *Mexicos climate change mid-century strategy.* Retrieved from https://unfccc.int/files/focus/long-term_strategies/application/pdf/mexico_mcs_final_cop22nov16_red.pdf

Silva, R. A., West, J. J., Zhang, Y., Anenberg, S. C., Lamarque, J.-F., Shindell, D. T., ... Zeng, G. (2013). Global premature mortality due to anthropogenic outdoor air pollution and the contribution of past climate change. *Environmental Research Letters*, *8*(3), 034005.

Smith, C. J., Kramer, R. J., Myhre, G., Forster, P. M., Soden, B. J., Andrews, T., ... Watson-Parris, D. (2018). Understanding rapid adjustments to diverse forcing agents. *Geophysical Research Letters*, *45*(21), 12,023-12,031. doi: 10.1029/2018GL079826

Smith, S. J., & Mizrahi, A. (2013). Near-term climate mitigation by short-lived forcers. *Proceedings of the National Academy of Sciences of the United States of America*, *110*(35), 14202-14206. doi: 10.1073/pnas.1308470110

Stevens, B., Giorgetta, M., Esch, M., Mauritsen, T., Crueger, T., Rast, S., ... Roeckner, E. (2013). Atmospheric component of the MPI-M Earth System Model: ECHAM6. *Journal of Advances in Modeling Earth Systems*, *5*(2), 146 - 172. Retrieved from http://search.ebscohost.com/login.aspx?direct=true&db=aph&AN=89241377&site=ehost-live

Stier, P., Feichter, J., Kinne, S., Kloster, S., Vignati, E., Wilson, J., ... Petzold, A. (2005). The aerosol-climate model ECHAM5-HAM. *Atmospheric Chemistry and Physics*, *5*(4), 1125–1156. Retrieved from https://

www.atmos-chem-phys.net/5/1125/2005/ doi: 10.5194/acp-5-1125-2005

Stjern, C. W., Samset, B. H., Myhre, G., Forster, P. M., Hodnebrog, Ø., Andrews, T., ... Voulgarakis, A. (2017). Rapid adjustments cause weak surface temperature response to increased black carbon concentrations. *Journal of Geophysical Research: Atmospheres*, *122*(21), 11,462-11,481. Retrieved from https://agupubs.onlinelibrary.wiley.com/doi/abs/10.1002/2017JD027326 doi: 10.1002/2017JD027326

Stohl, A., Aamaas, B., Amann, M., Baker, L. H., Bellouin, N., Berntsen, T. K., ... Zhu, T. (2015). Evaluating the climate and air quality impacts of short-lived pollutants. *Atmospheric Chemistry and Physics*, *15*(18), 10529.

Sun, J., Zhang, K., Wan, H., Ma, P.-L., Tang, Q., & Zhang, S. (2019). Impact of nudging strategy on the climate representativeness and hindcast skill of constrained EAMv1 simulations. *Journal of Advances in Modeling Earth Systems*, *11*(12), 3911-3933. Retrieved from https://agupubs.onlinelibrary.wiley.com/doi/abs/10.1029/2019MS001831 doi: 10.1029/2019MS001831

Taylor, K. E., Stouffer, R. J., & Meehl, G. A. (2012). An overview of CMIP5 and the experiment design. *Bulletin of the American Meteorological Society*, *93*(4), 485-498. doi: 10.1175/BAMS-D-11-00094.1

Tegen, I., Neubauer, D., Ferrachat, S., Siegenthaler-Le Drian, C., Bey, I., Schutgens, N., ... Lohmann, U. (2019). The global aerosol–climate model ECHAM6.3–HAM2.3 – part 1: Aerosol evaluation. *Geoscientific Model Development*, *12*(4), 1643–1677. Retrieved from https://www.geosci-model-dev.net/12/1643/2019/ doi: 10.5194/gmd-12-1643-2019

Thomson, A. M., Calvin, K. V., Smith, S. J., Kyle, G. P., Volke, A., Patel, P., ... Edmonds, J. A. (2011, Jul 29). RCP4.5: a pathway for stabilization of radiative forcing by 2100. *Climatic Change*, *109*(1), 77. Retrieved from https://doi.org/10.1007/s10584-011-0151-4 doi: 10.1007/s10584-011-0151-4

Trstl, J., Chuang, W. K., Gordon, H., Heinritzi, M., Yan, C., Molteni, U., ... Baltensperger, U. (2016). The role of low-volatility organic compounds in initial particle growth in the atmosphere. *Nature*, *533*(7604), 527-531. Retrieved from https://doi.org/10.1038/nature18271 doi: 10.1038/nature18271

Twomey, S. (1977). The influence of pollution on the shortwave albedo of clouds. *Journal of the Atmospheric Sciences*, *34*(7), 1149-1152. doi: 10.1175/1520-0469(1977)034⟨1149:TIOPOT⟩2.0.CO;2

UNEP. (2011). *Near-term climate protection and clean air benefits: Actions for controlling short-lived climate forcers.* Retrieved from http://hdl.handle.net/20.500.11822/8048

van Vuuren, D. P., Edmonds, J., Kainuma, M., Riahi, K., Thomson, A., Hibbard, K., ... Rose, S. K. (2011, Aug 05). The representative concentration pathways: an overview. *Climatic Change*, *109*(1), 5. Retrieved from https://doi.org/10.1007/s10584-011-0148-z doi: 10.1007/s10584-011-0148-z

Wang, Z. L., Zhang, H., & Zhang, X. Y. (2015). Simultaneous reductions in emissions of black carbon and co-emitted species will weaken the aerosol net cooling effect. *Atmospheric Chemistry and Physics*, *15*(7), 3671–3685. Retrieved from https://www.atmos-chem-phys.net/15/3671/2015/ doi: 10.5194/acp-15-3671-2015

WHO. (2019). *Ambient (outdoor) air quality and health fact sheet.* Retrieved from https://www.who.int/en/news-room/fact-sheets/detail/ambient-(outdoor)-air-quality-and-health.

Wood, R. (2012). Stratocumulus clouds. *Monthly Weather Review*, *140*(8), 2373-2423. Retrieved from https://doi.org/10.1175/MWR-D-11-00121.1 doi: 10.1175/MWR-D-11-00121.1

Wood, R., Mechoso, C. R., Bretherton, C. S., Weller, R. A., Huebert, B., Straneo, F., ... Bower, K. N. (2011). The VAMOS ocean-cloud-atmosphere-land study regional experiment (VOCALS-REx): goals, platforms, and field

operations. *Atmospheric Chemistry and Physics*, *11*(2), 627–654. Retrieved from https://www.atmos-chem-phys.net/11/627/2011/ doi: 10.5194/acp-11-627-2011

World Bank. (2020). *World Bank open data database.* Retrieved from https://data.worldbank.org/

Yang, Y., Smith, S. J., Wang, H., Mills, C. M., & Rasch, P. J. (2019). Variability, timescales, and nonlinearity in climate responses to black carbon emissions. *Atmospheric Chemistry and Physics*, *19*(4), 2405–2420. Retrieved from https://www.atmos-chem-phys.net/19/2405/2019/ doi: 10.5194/acp-19-2405-2019

Zarzycki, C. M., & Bond, T. C. (2010). How much can the vertical distribution of black carbon affect its global direct radiative forcing? *Geophysical Research Letters*, *37*(20). Retrieved from https://agupubs.onlinelibrary.wiley.com/doi/abs/10.1029/2010GL044555 doi: 10.1029/2010GL044555

Zhang, K., Wan, H., Liu, X., Ghan, S. J., Kooperman, G. J., Ma, P.-L., ... Lohmann, U. (2014). Technical note: On the use of nudging for aerosol-climate model intercomparison studies. *Atmospheric Chemistry and Physics*, *14*(16), 8631–8645. Retrieved from https://www.atmos-chem-phys.net/14/8631/2014/ doi: 10.5194/acp-14-8631-2014

Figure 1.

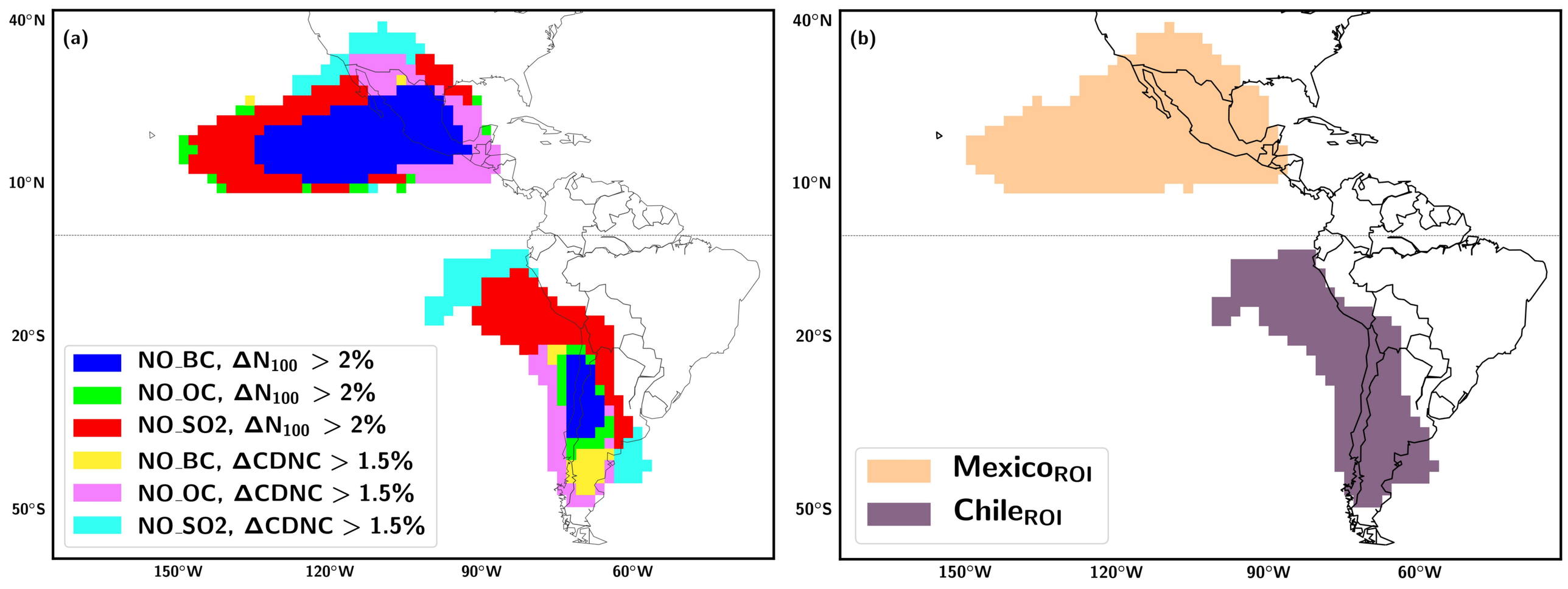
(a)
40°N
10°N
20°S
50°S
150°W
120°W
90°W
60°W
NO_BC, ΔN100 > 2%
NO_OC, ΔN100 > 2%
NO_SO2, ΔN100 > 2%
NO_BC, ΔCDNC > 1.5%
NO_OC, ΔCDNC > 1.5%
NO_SO2, ΔCDNC > 1.5%
(b)
40°N
10°N
20°S
50°S
150°W
120°W
90°W
60°W
MexicoROI
ChileROI

Figure 2.

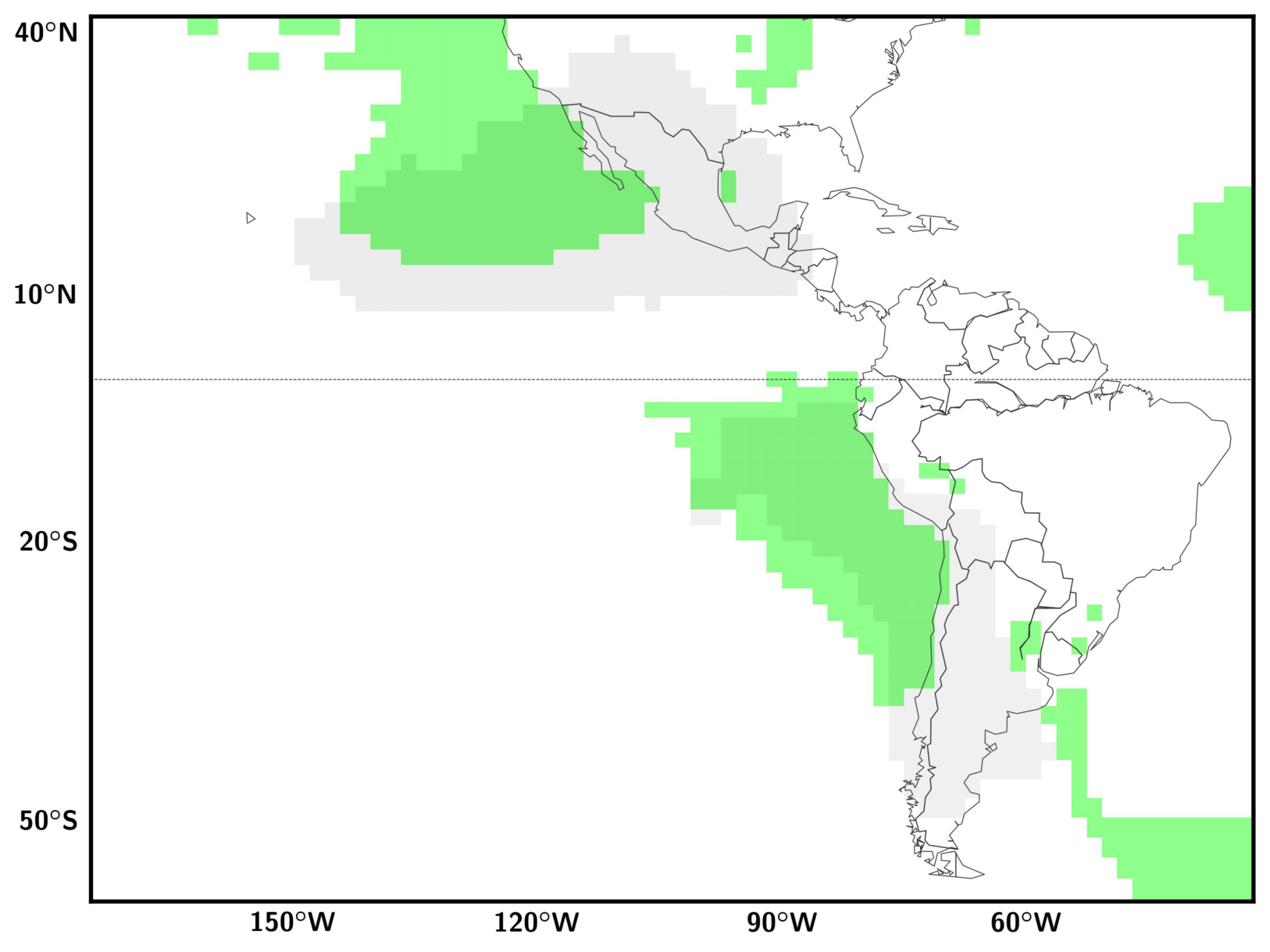
40°N
10°N
20°S
50°S
150°W
120°W
90°W
60°W

Figure 3.

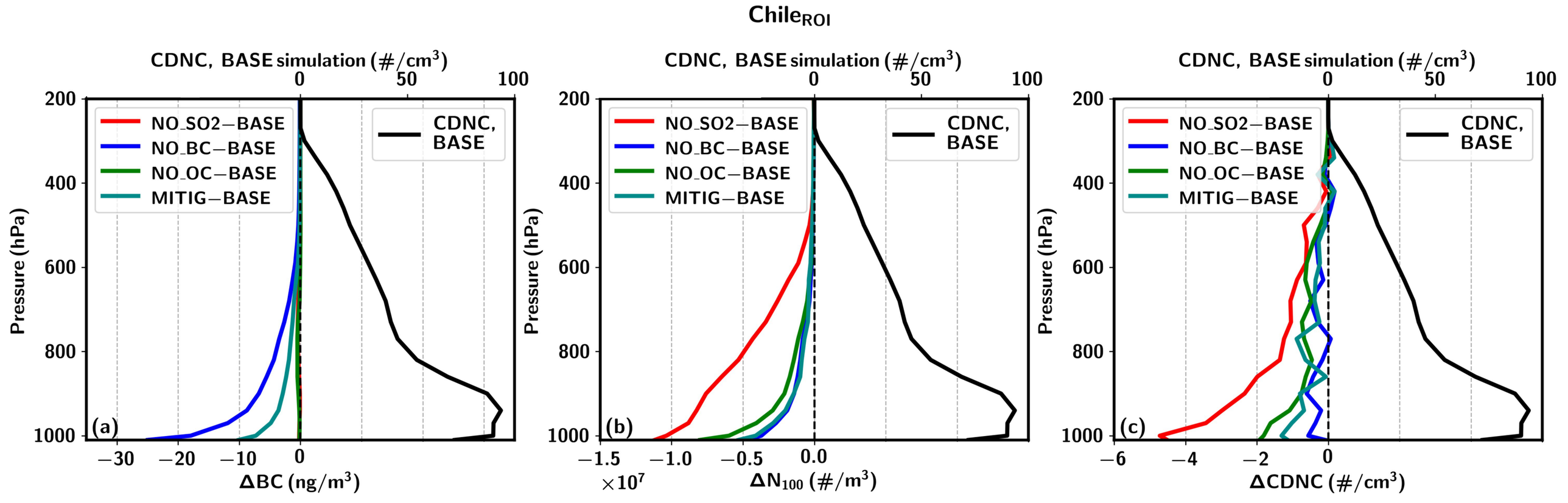
Chile$_{ROI}$
CDNC, BASE simulation (#/cm^3)
0
50
100
200
400
600
800
1000
Pressure (hPa)
NO_SO2−BASE
NO_BC−BASE
NO_OC−BASE
MITIG−BASE
CDNC, BASE
(a)
−30
−20
−10
0
ΔBC (ng/m^3)
(b)
−1.5
−1.0
−0.5
0.0
×10^7
ΔN$_{100}$ (#/m^3)
(c)
−6
−4
−2
ΔCDNC (#/cm^3)

Figure 4.

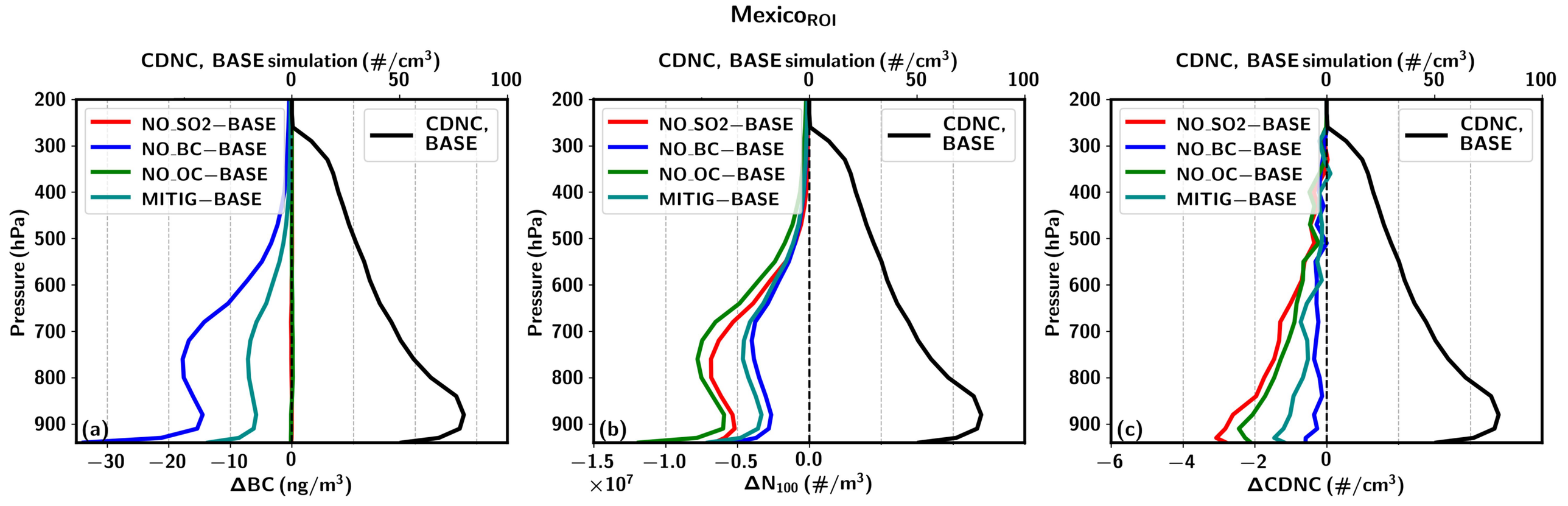
Mexico$_{ROI}$
CDNC, BASE simulation (#/cm^3)
0
50
100
200
300
400
500
600
700
800
900
Pressure (hPa)
NO_SO2−BASE
NO_BC−BASE
NO_OC−BASE
MITIG−BASE
CDNC, BASE
(a)
−30
−20
−10
0
ΔBC (ng/m^3)
(b)
−1.5
−1.0
−0.5
0.0
×10^7
ΔN$_{100}$ (#/m^3)
(c)
−6
−4
−2
0
ΔCDNC (#/cm^3)

Figure 5.

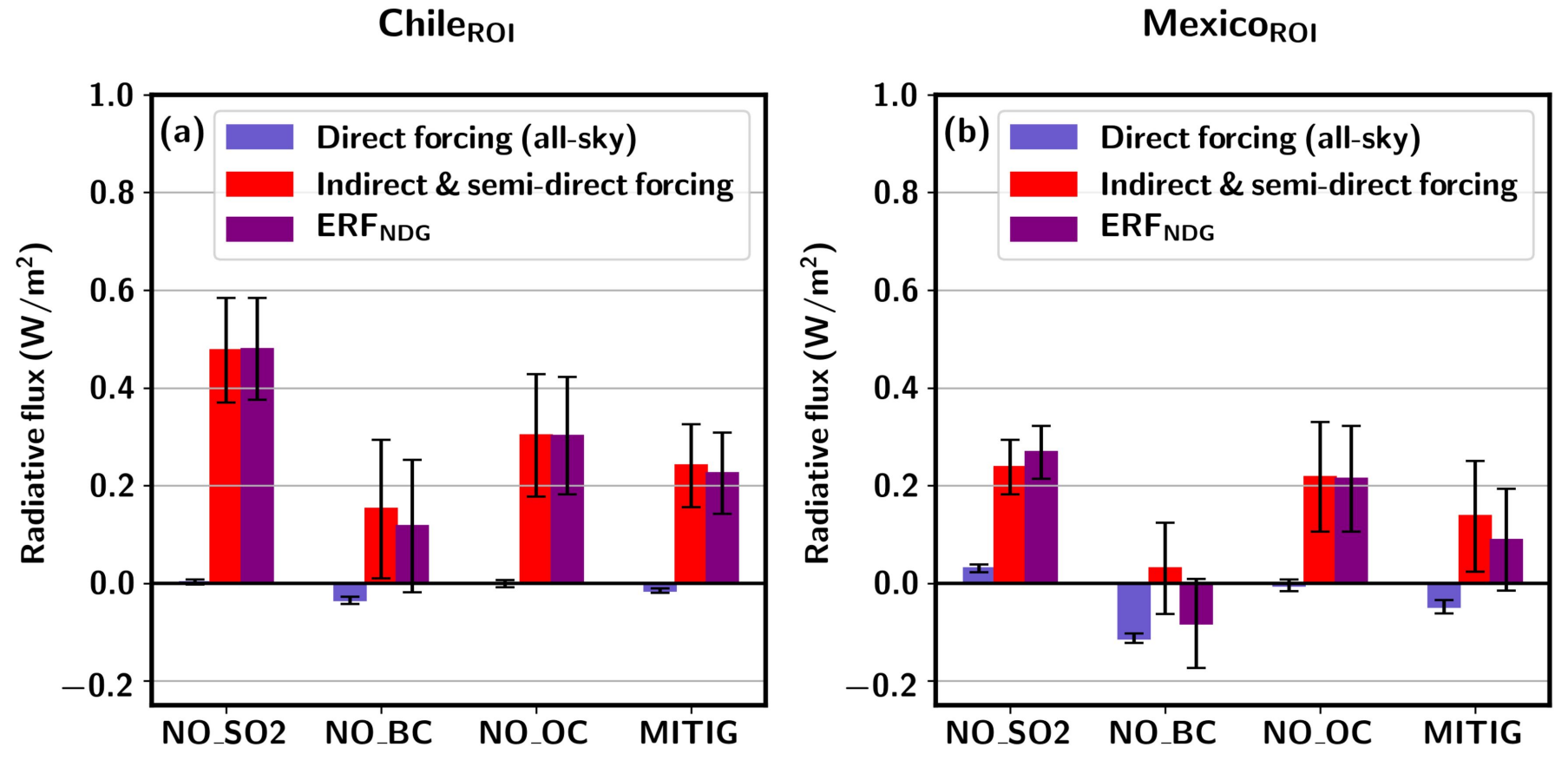
Chile$_{ROI}$
Mexico$_{ROI}$
(a)
(b)
Direct forcing (all-sky)
Indirect & semi-direct forcing
ERF$_{NDG}$
Radiative flux (W/m^2)
1.0
0.8
0.6
0.4
0.2
0.0
−0.2
NO_SO2
NO_BC
NO_OC
MITIG

Figure A1.

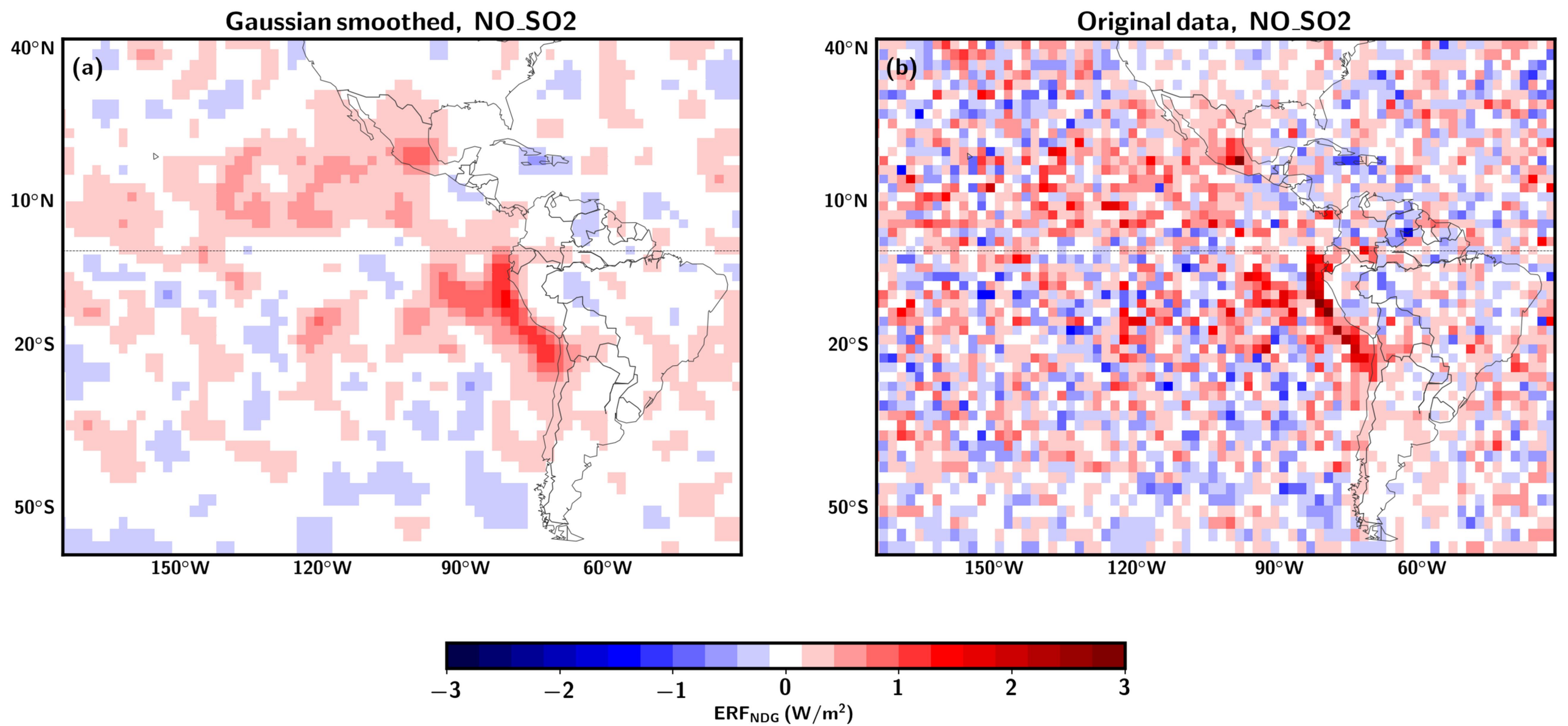
Gaussian smoothed, NO_SO2
Original data, NO_SO2
(a)
(b)
40°N
10°N
20°S
50°S
150°W
120°W
90°W
60°W
−3
−2
−1
0
1
2
3
ERF$_{NDG}$ (W/m^2)

Figure B1.

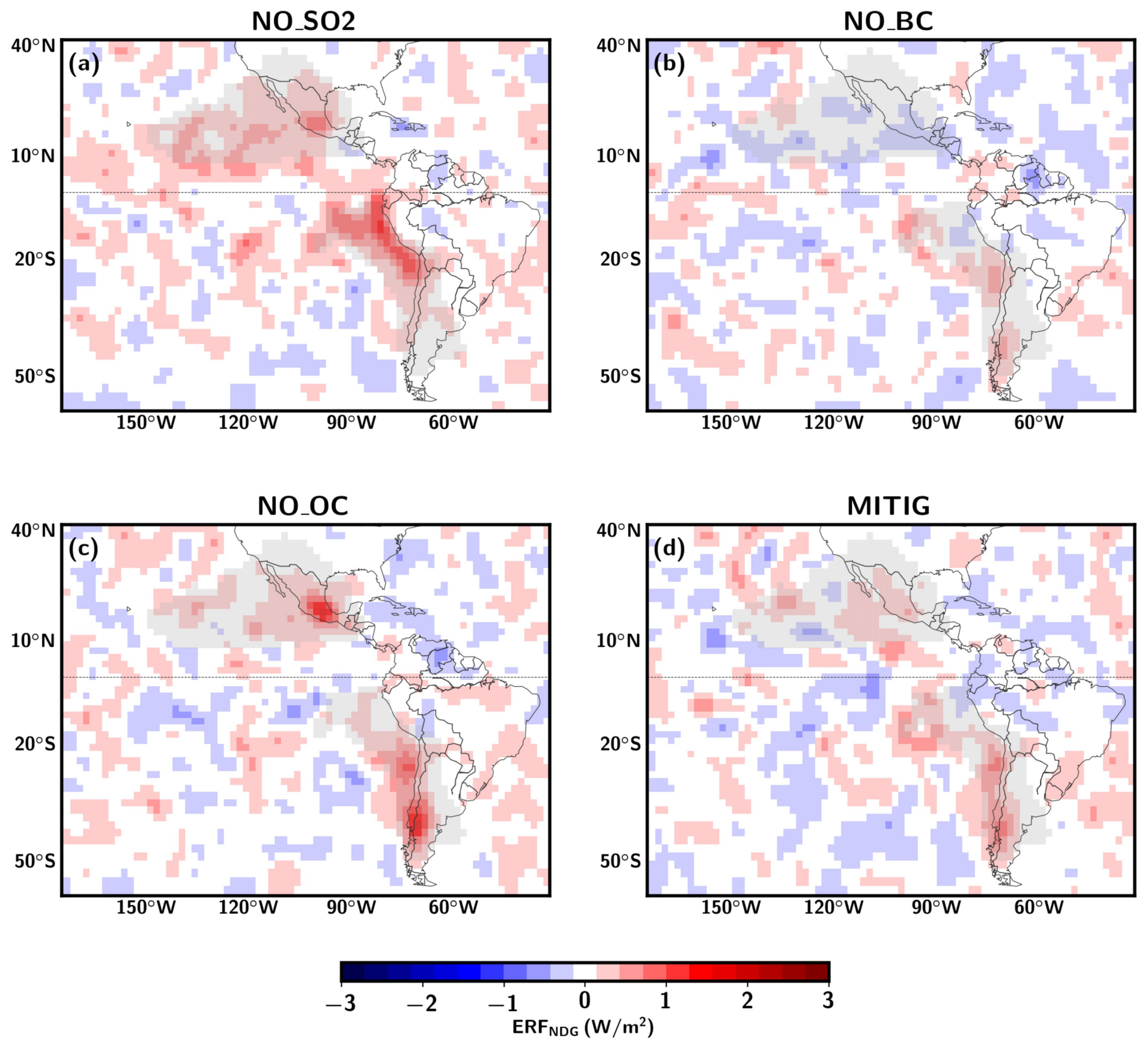
NO_SO2
(a)
NO_BC
(b)
NO_OC
(c)
MITIG
(d)
40°N
10°N
20°S
50°S
150°W
120°W
90°W
60°W
−3
−2
−1
0
1
2
3
ERF$_{NDG}$ (W/m^2)